

# A sequential ensemble approach to epidemic modeling: Combining Hawkes and SEIR models using SMC<sup>2</sup>

Dhorasso Temfack and Jason Wyse

*School of Computer Science and Statistics, Trinity College Dublin, Ireland*

June 19, 2025

## Abstract

This paper proposes a sequential ensemble methodology for epidemic modeling that integrates discrete-time Hawkes processes (DTHP) and Susceptible-Exposed-Infectious-Removed (SEIR) models. Motivated by the need for accurate and reliable epidemic forecasts to inform timely public health interventions, we develop a flexible model averaging (MA) framework using Sequential Monte Carlo Squared. While generating estimates from each model individually, our approach dynamically assigns them weights based on their incrementally estimated marginal likelihoods, accounting for both model and parameter uncertainty to produce a single ensemble estimate. We assess the methodology through simulation studies mimicking abrupt changes in epidemic dynamics, followed by an application to the Irish influenza and COVID-19 outbreaks. Our results show that combining the two models can improve both estimates of the infection trajectory and reproduction number compared to using either model alone. Moreover, the MA consistently produces more stable and informative estimates of the time-varying reproduction number, with credible intervals that maintain appropriate coverage. These features are particularly valuable in high-uncertainty contexts where reliable situational awareness is essential. This research contributes to pandemic preparedness by enhancing forecast reliability and supporting more informed public health responses.

**Keywords:** Sequential Monte Carlo Squared, Bayesian model averaging, SEIR model, Discrete-time Hawkes Process

## 1 Introduction

Emerging infectious diseases pose significant challenges to public health systems worldwide. In situations where no effective vaccine is available, governments must rapidly implement a range of non-pharmaceutical interventions (NPIs) to mitigate the spread of the virus. From social distancing measures to intensive lockdowns, these strategies are often guided by mathematical and statistical models (Hellewell et al., 2020; Fowler et al., 2020). Statistical models enable policymakers to simulate multiple scenarios and quantify the efficacy of interventions, thus informing decisions aimed at minimizing the burden on healthcare systems.

Among the most widely adopted frameworks are compartmental models, such as the SIR (Susceptible-Infectious-Removed) or SEIR (Susceptible-Exposed-Infectious-Removed) model, which provide an intuitive representation of disease dynamics by tracking transitions between health states (Kermack and McKendrick, 1927). Compartmental models are typically described by a system of equations that govern the rates at which individuals move between compartments based on disease-specific parameters. A widely used approach for estimating the parameters of such models is Bayesian inference, which provides a principled way to quantify uncertainty in model estimates and incorporate prior knowledge. SEIR-type models have been extensively applied to various infectious diseases, including

Ebola (Lekone and Finkenstädt, 2006; Funk et al., 2018), Influenza (Dureau et al., 2013; Birrell et al., 2020), and COVID-19 (Cazelles et al., 2021; Storvik et al., 2023). Their modular structure also makes them easily extendable to incorporate additional compartments or features, such as vaccination, age structure, or spatial dynamics. Moreover, they enable the estimation of key epidemiological quantities, such as the incubation and infectious periods, which are directly interpretable by epidemiologists. However, increasing model complexity can introduce challenges, including parameter identifiability issues, potential biases, and susceptibility to mis-specification, all of which require careful consideration during model development and inference (Kresin et al., 2021). In response, researchers have explored alternative modeling frameworks, including point process models such as the Hawkes process.

The Hawkes process (Hawkes, 1971) is a type of self-exciting point process where past events influence the likelihood of future occurrences. This model has gained attention for its ability to capture event clustering and self-excitation, making it particularly suitable for modeling infectious disease case series. A notable early use of point process models for infectious diseases, though not Hawkes-based was by Meyer and Held (2014). The first Hawkes-based application to real outbreak data was proposed by Kelly et al. (2019), who developed a nonparametric model to forecast the 2018–2019 Ebola outbreak in the Democratic Republic of the Congo. During the COVID-19 pandemic, Hawkes processes were employed to estimate the time-evolution of the reproduction number (Mohler et al., 2021; Chiang et al., 2022; Lamprinakou et al., 2023). Several studies have compared Hawkes processes with compartmental models. Bertozzi et al. applied a continuous-time Hawkes model to COVID-19 data in U.S. states, but it underperformed relative to traditional SIR/SEIR models during early epidemic phases. In contrast, Kresin et al. (2021) reported that the Hawkes process outperformed SEIR, reducing forecast error by 20–30% in most cases. These comparisons often used deterministic SEIR-type models, which may partly explain the relative success of Hawkes approaches. The discrete-time Hawkes process (DTHP), in particular, benefits from structural simplicity and reduced risk of model misspecification. Park et al. (2022) found that a Hawkes model improved forecasts by 38% over SEIR during the 2014–2016 Ebola outbreak. Furthermore, Rizoïu et al. (2018) introduced the HawkesN process, bridging Hawkes and SIR frameworks by incorporating finite population constraints. They showed that, in the absence of background events and assuming an exponential infectious period, the expected conditional intensity of HawkesN matches that of the stochastic SIR model, providing a mechanistic link between these approaches.

Unlike compartmental models, the Hawkes process models infections using a single conditional intensity function, avoiding assumptions about unobserved states. However, in real-world scenarios, the exact timing of each infection is rarely recorded. Instead, data are reported in aggregated time intervals (e.g., daily or weekly). To address this, the discrete-time Hawkes process (DTHP) was developed to accommodate aggregate case data without requiring artificial interpolation of infection times. This approach has been applied in various contexts, including modeling the spread of COVID-19 (Browning et al., 2021; Koyama et al., 2021).

Having access to appropriate modeling and prediction techniques during an emerging outbreak is critical, as their outputs can play a prominent role in policy decisions and intervention strategies. A common approach is to assume the data follows one specific model. To address this limitation, we propose an ensemble modeling framework that integrates estimates from both the DTHP and a stochastic SEIR model, accounting for uncertainty in both model structure and parameters. We employ the Sequential Monte Carlo Squared (SMC<sup>2</sup>) algorithm of Chopin et al. (2013), adapted to jointly estimate the latent states and parameters of each model. By weighting model outputs based on their predictive performance, we dynamically combine their estimates. Our approach focuses on online inference of the case incidence and the instantaneous reproduction across models.

While Bayesian model averaging is well-established in infectious disease modeling (Castañeda and Aerts, 2015; Park et al., 2017; Goudie et al., 2019), most existing approaches rely on MCMC methods to compute posterior model probabilities. These require access to the full dataset, rendering them impractical for real-time applications. To address this, Bayesian model averaging using SMC methods has been proposed to sequentially integrate predictions from multiple models, weighted by their posterior likelihoods of generating observed data (Parrish et al., 2012; Rings et al., 2012; Martino et al., 2015; Urteaga et al., 2016), though these approaches have not yet been applied to epidemiological modeling. Moreover, they typically assume known model parameters, neglecting internal parameter uncertainty, a condition rarely met in practice. Our work builds on and extends these efforts by embedding Bayesian model averaging within the SMC<sup>2</sup> framework to jointly infer states and parameters from DTHP and SEIR models in real time. Rather than treating models in isolation and aggregating results post hoc, our framework integrates them within a unified inference procedure, allowing both models to run in “parallel” while dynamically fusing their common estimates at each time step, thus addressing both model and parameter uncertainty to support robust real-time decision-making during outbreaks. enables more coherent handling of model and parameter uncertainty, ultimately supporting robust decision-making during outbreaks. A valuable byproduct of this approach is the ability to estimate key epidemiological quantities, such as the infectious period from the SEIR model, and to assess how past events influence current transmission dynamics via the DTHP triggering kernel, providing complementary insights alongside primary predictions.

The remainder of this paper is structured as follows: In Section 2, we define the DTHP and stochastic SEIR models employed in this study. Section 3 describes the Bayesian model averaging approach and the sequential estimation procedure using SMC<sup>2</sup>. Section 4 presents detailed results, including the experimental setup and analysis of real data from the Irish influenza and COVID-19 epidemics. Finally, Section 5 concludes with a summary of our findings and their implications for future research.

## 2 Statistical models

A key metric of transmissibility in infectious diseases is the time-varying reproduction number  $R_t$ , which reflects the average number of secondary infections arising from an infected individual at time  $t$  in a population where some individuals are immune or other interventions have been implemented. Monitoring  $R_t$  provides real-time insights into the dynamics of an epidemic. If  $R_t > 1$ , the number of infections is likely to increase. Conversely, if  $R_t < 1$ , the epidemic is expected to decline over time. This makes  $R_t$  an essential tool for assessing the effectiveness of control measures and guiding public health decisions. Due to the dynamic and uncertain nature of infectious disease transmission, it is crucial to employ statistical models that can effectively capture these complexities. In this study, we propose a hybrid approach that combines two well-established models: the Discrete-Time Hawkes Process and the stochastic SEIR model. These models were selected for their balance of simplicity and their ability to represent the stochasticity inherent in transmission dynamics.

### 2.1 Discrete-Time Hawkes Process

The Discrete-Time Hawkes Process (DTHP) is a stochastic point process specifically designed to model the occurrence of events such as new cases of an infectious disease over discrete time intervals (Koyama et al., 2021; Browning et al., 2021). This model extends the continuous-time Hawkes process when the exact timing of each infection is unknown. Mathematically, the DTHP model is characterized by a conditional intensity function  $\lambda_H(t)$ , which represents the expected number of cases occurring at time  $t$ , given the history of previous cases. Unlike the continuous-time formulation, where the event history  $\mathcal{H}_{t-1}$  typically consists of precise event times and associated marks, the discrete-time version uses

only aggregated past counts. Specifically, the history is given by  $\mathcal{H}_{t-1} := \{y_s | 1 \leq s \leq t-1\}$ , where  $y_s$  denotes the number of cases observed at time  $s$ . The model is defined as follows:

$$\mathcal{M}_1 : \begin{cases} \lambda_H(t) = \left(1 - \frac{\sum_{s=1}^{t-1} y_s}{N}\right) \left[\mu + R_t \sum_{s=1}^{t-1} y_s \varphi_{t-s}\right], \\ \log(R_t) = \log(R_{t-1}) + \varepsilon_{1,t}, \quad \varepsilon_{1,t} \sim \mathcal{N}(0, \nu_1^2) \end{cases}, \quad (1)$$

Here  $\mu$  represents the expected number of spontaneous or imported cases. The term  $\sum_{s=1}^{t-1} y_s \varphi_{t-s}$  captures the cumulative self-excitation process, the mechanism by which  $y_s$  cases that occurred at time  $s$  exert influence with a delay of  $t-s$  unit of time. The function  $\varphi_{t-s}$  is the triggering kernel, describing the discrete distribution of the delay  $d = t-s$  between infection and subsequent transmission and satisfies  $\sum_{d=1}^{\infty} \varphi_d = 1$ . We adopt a geometric kernel, defined as  $\varphi_d = \omega(1-\omega)^{d-1}$ . This choice is motivated by the relationship between the geometric and exponential distributions: in continuous-time Hawkes processes, the exponential kernel is widely used to model memory decay. The geometric distribution can be seen as its natural discrete-time counterpart, offering a conceptually equivalent representation of how infectiousness decays over time (Browning et al., 2021). In this context  $\omega \in (0, 1)$  controls the rate at which the influence of past cases diminishes over time. The factor  $\left(1 - \frac{\sum_{s=1}^{t-1} y_s}{N}\right)$  accounts for the reduction in the susceptible population due to prior infections, ensuring that the model reflects the decreasing pool of individuals at risk as the epidemic progresses;  $N$  denotes the total population size. Since the true trajectory of the reproduction number  $R_t$  is unknown and likely to change over time due to interventions or behavioral shifts, we model  $\log(R_t)$  as a random walk. This flexible formulation allows  $R_t$  to adapt dynamically to change and seems more suited than a stationary process, which implies time-invariant statistical properties. The log-transform ensures positivity of  $R_t$ , a biologically meaningful constraint. This approach is widely adopted in both continuous and discrete-time epidemic models (Abbott et al., 2020; Koyama et al., 2021; Lamprinakou et al., 2023). We ensure numerical stability by placing a prior on  $\nu_1$  that encourages small variability, thereby penalizing against runaway growth in  $R_t$ .

## 2.2 Stochastic SEIR model

The stochastic SEIR model provides a framework for characterizing transitions between different stages of an epidemic. Susceptible individuals become exposed upon contact with infectious individuals. Exposed individuals transition to the infectious state after an incubation delay, and infectious individuals are eventually removed through recovery or death. The number of individuals transitioning between compartments are modeled as binomial random variables. The model is defined by the following update equations, based on Lekone and Finkenstädt (2006):

$$\mathcal{M}_2 : \begin{cases} S(t+1) = S(t) - \lambda_{SE}(t), & \lambda_{SE}(t) \sim \text{Binomial}\left(S(t), 1 - e^{-\beta t \frac{I(t)}{N}}\right), \\ E(t+1) = E(t) + \lambda_{SE}(t) - \lambda_{EI}(t), & \lambda_{EI}(t) \sim \text{Binomial}\left(E(t), 1 - e^{-\sigma}\right), \\ I(t+1) = I(t) + \lambda_{EI}(t) - \lambda_{IR}(t), & \lambda_{IR}(t) \sim \text{Binomial}\left(I(t), 1 - e^{-\gamma}\right), \\ R(t+1) = R(t) + \lambda_{IR}(t), \\ \log(\beta_t) = \log(\beta_{t-1}) + \varepsilon_{2,t}, & \varepsilon_{2,t} \sim \mathcal{N}(0, \nu_2^2), \\ R_t = \frac{\beta_t}{\gamma}. \end{cases} \quad (2)$$

In this model,  $S(t)$ ,  $E(t)$ ,  $I(t)$ , and  $R(t)$  represent the numbers of susceptible, exposed (infected but not yet infectious), infectious, and removed (recovered or dead) individuals at time  $t$ , respectively. We assume a closed population, i.e.  $N = S(t) + E(t) + I(t) + R(t)$  for all  $t \in \mathbb{N}$ . While the classic SEIR model with constant parameters provides a useful

baseline for understanding epidemic dynamics, it is structurally limited in its ability to capture complex phenomena such as multiple waves of infection. To overcome this, we augment the model with a time-varying transmission rate  $\beta_t$ , which evolves according to a log-normal random walk, analogous to the modeling of  $R_t$  in DTHP discussed above. The parameters  $1/\sigma$  and  $1/\gamma$  represent the average durations of the latent and infectious periods, respectively. The quantities  $\lambda_{SE}(t)$ ,  $\lambda_{EI}(t)$ , and  $\lambda_{IR}(t)$  represent new exposures, new infections, and recoveries, while  $R_t$  denotes the time-varying reproduction number.

Both the DTHP and SEIR models incorporate a random walk process, which allows for a flexible representation of the dynamics of  $R_t$ . The volatility parameters  $\nu_k$ , for  $k = 1, 2$ , govern the magnitude of these fluctuations and are estimated sequentially from the observed data using the SMC<sup>2</sup> algorithm discussed in Section 2. Intuitively, higher values of  $\nu_k$  correspond to larger fluctuations in  $R_t$  over time. As demonstrated in Section 4, this simplified approach enables accurate tracking of the reproduction number using only the observed incidence data. Other extensions of the SEIR model are also possible and are discussed and analysed later on.

### 2.3 Observation process

Let  $y_t$  denote the number of observed cases on day  $t = 1, \dots, T$ . To link  $y_t$  with the expected number of new infections in model  $\mathcal{M}_k$ , we define the function:

$$\lambda_k(t) = \begin{cases} \lambda_H(t), & \text{DTHP model if } k = 1, \\ \lambda_{EI}(t), & \text{SEIR model if } k = 2. \end{cases} \quad (3)$$

During an epidemic, daily reported case counts are subject to various sources of noise, including measurement error, behavioral factors, and inherent randomness. To account for this, we model the observed case counts using a negative binomial distribution (Koyama et al., 2021; Inouzhe et al., 2023), with mean  $\lambda_k(t)$  and variance  $\lambda_k(t) + \phi_k \lambda_k^2(t)$ , where  $\phi_k > 0$  is an overdispersion parameter, i.e.,

$$y_t | \lambda_k(t) \sim \text{NegBin}(\lambda_k(t), \lambda_k(t) + \phi_k \lambda_k^2(t)), \quad k \in \{1, 2\}, \quad (4)$$

with a probability mass function

$$g(y_t | \lambda_k(t), \phi_k) = \frac{\Gamma(y_t + \frac{1}{\phi_k})}{y_t! \Gamma(\frac{1}{\phi_k})} \left( \frac{1}{1 + \phi_k \lambda_k(t)} \right)^{\frac{1}{\phi_k}} \left( \frac{\phi_k \lambda_k(t)}{\phi_k \lambda_k(t) + 1} \right)^{y_t}, \quad k \in \{1, 2\}. \quad (5)$$

As  $\phi_k$  tends to 0, the variance approaches the mean, and we have convergence to a Poisson probability mass function. The negative binomial distribution is widely used to accommodate overdispersed count data, providing a more flexible fit than the Poisson distribution in such contexts (Lindén and Mäntyniemi, 2011). Importantly, this formulation assumes perfect case detection and does not explicitly account for case ascertainment fractions or reporting delays. However, for more practical applications, such factors can easily be incorporated into the model through additional latent processes or delay distributions (Birrell et al., 2017; Abbott et al., 2020).

## 3 Sequential Bayesian inference and Bayesian model averaging

SMC-based methods facilitate approximate inference in Bayesian sequential models by representing the evolving posterior over latent states through a set of weighted particles, making them well-suited for real-time data assimilation. Building on this, model averaging combines predictions from multiple candidate models, weighting them by their posterior model probabilities obtained via the SMC framework (Martino et al., 2015; Urteaga et al., 2016). This approach incorporates model uncertainty into the analysis, resulting in more robust and reliable predictions.

### 3.1 State-space formulation

Assume the observed data is generated by one of the candidate models  $\mathcal{M}_k$ , where  $k \in \{1, 2\}$ . In this study, we adopt the following state-space formulation (Jacob et al., 2017) to describe the latent state and observation processes at discrete times  $t = 1, \dots, T$ :

$$x_{k,0} \sim f_k(x_{k,0}|\theta_k), \quad \triangleright \text{Initial state} \quad (6)$$

$$x_{k,t}|x_{k,0:t-1} \sim f_k(x_{k,t}|x_{k,0:t-1}, \theta_k), \quad \triangleright \text{State process} \quad (7)$$

$$y_t|x_{k,t} \sim g(y_t|x_{k,t}, \theta_k), \quad \triangleright \text{Observation process} \quad (8)$$

where the latent state  $x_{k,t} \in \mathbb{R}^{n_{x_k}}$  is propagated according to the transition density  $f_k(x_{k,t}|x_{k,0:t-1}, \theta_k)$ , which is simply one of the statistical models given in Equations (1) and (2). The observations  $y_t \in \mathbb{R}$  are linked to the latent states through the emission density  $g(y_t|x_{k,t}, \theta_k)$ , as in Equation (5) and the vectors  $\theta_k \in \Theta_k \subset \mathbb{R}^{n_{\theta_k}}$  represent static parameters in the corresponding model. For any sequence  $\{z_t\}_{t \geq 0}$ , we denote  $z_{i:j} = \{z_i, z_{i+1}, \dots, z_j\}$ .

When  $k = 1$ , the state-space model corresponds to the DTHP model, as given in (1), with the latent state  $x_{1,t} = (\lambda_H(t), R_t)$  and parameters  $\theta_1 = (\mu, \omega, \nu_1, \phi_1)$ .

For  $k = 2$ , it corresponds to the SEIR model, as given in (2), with the latent state  $x_{2,t} = (S(t), E(t), I(t), R(t), \lambda_{EI}(t), R_t)$  and parameters  $\theta_2 = (\sigma, \gamma, \nu_2, \phi_2)$ .

In each case, inference is performed on the sequence of latent variables  $x_{k,t}$  giving the observation  $y_{1:t}$  by using the posterior distribution  $p(x_{k,t}|y_{1:t}, \theta_k, \mathcal{M}_k)$ . Bayesian model averaging provides a formal probabilistic framework for obtaining predictive inference on quantities of interest that are not model-specific (Hoeting et al., 1999). Specifically, the posterior distribution of a quantity of interest at time  $t$ , denoted  $\Delta_t$ , which has a consistent interpretation across all considered models (in our context,  $\Delta_t$  is the expected newly infected cases or the time-varying reproduction number), can be expressed as a weighted mixture of the model-specific posterior distributions:

$$p(\Delta_t|y_{1:t}) = \pi_{1,t}p(\Delta_t|y_{1:t}, \theta_1, \mathcal{M}_1) + \pi_{2,t}p(\Delta_t|y_{1:t}, \theta_2, \mathcal{M}_2), \quad (9)$$

where the coefficients  $\pi_{k,t}$ ,  $k = 1, 2$  are the posterior model probabilities that reflect the relative credibility of each model given the observed data  $y_{1:t}$  and expressed as:

$$\pi_{k,t} := p(\mathcal{M}_k|y_{1:t}) = \frac{p(y_{1:t}|\theta_k, \mathcal{M}_k)p(\mathcal{M}_k)}{\sum_{j=1}^2 p(y_{1:t}|\theta_j, \mathcal{M}_j)p(\mathcal{M}_j)}, \quad \text{for } k = 1, 2. \quad (10)$$

Here,  $p(y_{1:t}|\theta_k, \mathcal{M}_k)$  is the model evidence:

$$p(y_{1:t}|\theta_k, \mathcal{M}_k) = \prod_{s=1}^t p(y_s|y_{1:s-1}, \theta_k, \mathcal{M}_k), \quad k = 1, 2. \quad (11)$$

The term  $p(y_s|y_{1:s-1}, \theta_k, \mathcal{M}_k)$  represents the incremental likelihood. The prior  $p(\mathcal{M}_k)$  reflects our prior belief in each model's ability to represent the observations. In this study, equal prior probabilities are assigned to each model,  $p(\mathcal{M}_1) = p(\mathcal{M}_2)$ , reflecting no a priori preference for either model.

### 3.2 Sequential Monte Carlo for known parameters

When the model parameters  $\theta_k$  are known, Sequential Monte Carlo (SMC), also referred to as particle filtering (Gordon et al., 1993; Doucet et al., 2001), recursively approximates the filtering distribution of the latent variables at each time point, given the data up to time  $t$ . This is achieved by sequentially generating a set of particles with associated weights, denoted by  $\{x_{k,t}^i, w_{k,t}^i\}_{i=1}^{N_x}$ , using importance sampling and resampling techniques. Here,  $N_x$  denotes the number of particles, and  $w_{k,t}^i$  represents the unnormalized importance weight of the  $i$ -th particle at time  $t$ , defined as:

$$w_{k,t}^i = w_{k,t-1}^i \frac{g(y_t|x_{k,t}^i, \theta) f_k(x_{k,t}^i|x_{k,0:t-1}^i, \theta)}{q_k(x_{k,t}^i|x_{k,0:t-1}^i, y_t, \theta)}, \quad i = 1, \dots, N_x, \quad (12)$$

where  $x_{k,t}^i$  is sampled from the importance distribution  $q_k(\cdot|x_{k,0:t-1}^i, y_t, \theta_k)$ . At each time  $t$ , the filtering distribution of the latent state can then be approximated by a weighted sum of Dirac delta functions:

$$p(x_{k,t}|y_{1:t}, \theta_k, \mathcal{M}_k) \approx \sum_{i=1}^{N_x} W_{k,t}^i \delta_{x_{k,t}^i}(x_{k,t}), \quad W_{k,t}^i = w_{k,t}^i / \sum_{j=1}^{N_x} w_{k,t}^j. \quad (13)$$

After the resampling step, the posterior distribution is approximated as:

$$p(x_{k,t}|y_{1:t}, \theta_k, \mathcal{M}_k) \approx \frac{1}{N_x} \sum_{i=1}^{N_x} \delta_{x_{k,t}^{a_t^i}}(x_{k,t}), \quad (14)$$

where  $a_t^i$  denotes the resampled ancestor index at time  $t$  (see Algorithm 1).

A notable particle filtering method employed in this study is the Bootstrap Particle Filter (BPF) (Gordon et al., 1993), which simplifies weight calculations by setting the importance distribution equal to the state transition distribution, i.e,  $q_k(x_{k,t}|x_{k,0:t-1}, y_t, \theta) = f_k(x_{k,t}|x_{k,0:t-1}, \theta)$ . The particle filter scheme (Algorithm 1) involves propagating many random realizations (particles) of the system state forward in time using the respective stochastic models (here, DTHP and SEIR models). Each particle is then assigned a weight proportional to the likelihood of its simulated observations matching the actual observed data.

---

**Algorithm 1** Bootstrap Particle Filter (BPF)

---

Operations involving index  $i$  must be performed for  $i = 1, \dots, N_x$ .

The indices  $a_t^{1:N_x}$  define the ancestral state particles at time  $t$  after the resampling.

**Inputs:** Observation:  $y_{1:T}$ , Number of particles:  $N_x$ , Initial state distribution:  $f_k(x_{k,0}|\theta_k)$ , Parameter vector:  $\theta_k$ .

**Output:** Particles set:  $\{x_{k,0:t}^i, w_{k,0:t}^i\}_{i=1}^{N_x}$ , marginal likelihood :  $\hat{p}_{N_x}(y_{1:t}|\theta_k, \mathcal{M}_k)$

---

- 1: Sample initial particles :  $x_{k,0}^i \sim f_k(x_{k,0}|\theta_k)$
  - 2: Compute weights:  $w_0^i = 1, \quad W_{k,0}^i = 1/N_x$
  - 3: **for**  $t = 1$  to  $T$  **do**
  - 4:   Sample new indices:  $a_t^{1:N_x} \sim \text{Resample}(W_{k,t-1}^{1:N_x})$
  - 5:   Propagate states  $x_{k,t}^i \sim f_k(\cdot|x_{k,0:t-1}^{a_t^i}, \theta_k)$
  - 6:   Compute weights and normalize:  $w_{k,t}^i = g(y_t|x_{k,t}^i, \theta_k), \quad W_{k,t}^i = w_{k,t}^i / \sum_{j=1}^{N_x} w_{k,t}^j$
  - 7:   Compute  $\hat{p}_{N_x}(y_{1:t}|\theta_k, \mathcal{M}_k)$  using Equation (17)
  - 8: **end for**
- 

In Algorithm 1, the resampling step, outlined in Step 4, eliminates particles with low weights and replicates those with higher weights. After resampling, all particle weights are reset to one. Unless stated otherwise, we employ stratified resampling throughout our implementations due to its efficiency and lower computational cost (Douc and Cappé, 2005; Vieira, 2018). Step 5 involves applying the transition density  $f_k$ , which corresponds to the state update rule of either the DTHP model (Equation (1)) or the SEIR model (Equation (2)). Step 6 entails evaluating the negative binomial probability mass function, as defined in Equation (5). In cases with missing observations, we set  $w_{k,t}^i = 1$ . A notable feature of particle filtering is that it provides an unbiased estimate of the incremental likelihood. Specifically, we have:

$$\begin{aligned} p(y_t|y_{1:t-1}, \theta, \mathcal{M}_k) &= \int g(y_t|x_{k,t}, \theta_k) p(x_{k,t}|y_{1:t-1}, \theta_k) dx_{k,t} \\ &= \mathbb{E}_{p(x_{k,t}|y_{1:t-1}, \theta_k)} [g(y_t|x_{k,t}, \theta_k)] \end{aligned} \quad (15)$$

and noting that in the case of the BPF, the weights are exactly  $w_t = g(y_t|x_{k,t}, \theta)$ , we can use the trajectories  $\{x_{k,t}^i\}_{i=1}^{N_x}$  sampled from the one-step-ahead predictive density  $p(x_{k,t}|y_{1:t-1}, \theta)$  and use a Monte Carlo approximation of the expectation to obtain:

$$\widehat{p}_{N_x}(y_t|y_{1:t-1}, \theta_k, \mathcal{M}_k) = \frac{1}{N_x} \sum_{i=1}^{N_x} w_{k,t}^i. \quad (16)$$

Hence, by the law of total probability, we can deduce the marginal likelihood up to the time  $t$  for a given  $\theta_k$  :

$$p(y_{1:t}|\theta_k, \mathcal{M}_k) \approx \widehat{p}_{N_x}(y_{1:t}|\theta_k, \mathcal{M}_k) = \prod_{s=1}^t \widehat{p}_{N_x}(y_s|y_{1:s-1}, \theta_k, \mathcal{M}_k) = \prod_{s=1}^t \left( \frac{1}{N_x} \sum_{i=1}^{N_x} w_{k,s}^i \right). \quad (17)$$

In many realistic situations, one does not know which parameter value  $\theta_k$  to plug into the model. While expert opinion can sometimes be relied upon to estimate epidemiological quantities such as the average infectious period, it is more challenging to select appropriate values for hyper-parameters governing the innovation of the Brownian process and the observation distribution. To learn about the parameters from the observations, a prior probability distribution  $p(\theta_k)$  is given to the parameter  $\theta_k$ , and the goal is to estimate the sequence of posterior distributions given the observations.

### 3.3 Sequential Monte Carlo Squared

SMC<sup>2</sup> targets the sequence of posterior distributions over parameters,  $\{p(\theta_k|y_{1:t}, \mathcal{M}_k), t = 1, \dots, T\}$  which evolve as new data becomes available. Given a prior density  $p(\theta_k)$  over the parameters  $\theta_k$ , Bayes' theorem gives:

$$\begin{aligned} p(\theta_k|y_{1:t}, \mathcal{M}_k) &= p(y_{1:t}|\theta_k, \mathcal{M}_k) p(\theta_k)/p(y_{1:t}, \mathcal{M}_k) \\ &= p(y_t|y_{1:t-1}, \theta_k, \mathcal{M}_k) p(\theta_k|y_{1:t-1}, \mathcal{M}_k) p(\theta_k)/p(y_{1:t}, \mathcal{M}_k) \\ &\propto p(y_t|y_{1:t-1}, \theta_k, \mathcal{M}_k) p(\theta_k|y_{1:t-1}, \mathcal{M}_k) \end{aligned} \quad (18)$$

Equation (18) suggests a sequential importance sampling approach. This involves reweighting a set of parameter particles based on the incremental likelihood  $p(y_t|y_{1:t-1}, \theta_k, \mathcal{M}_k)$ .

For each of the  $N_\theta$   $\theta$ -particles,  $\{\theta_{k,t}^m, \omega_{k,t}^m\}_{m=1}^{N_\theta}$  from  $p(\theta_k|y_{1:t}, \mathcal{M}_k)$ , we associate  $N_x$   $x$ -particles and perform the BPF. The SMC<sup>2</sup> algorithm reweights each  $\theta$ -particle according to an unbiased estimate of the incremental likelihood  $p(y_t|y_{1:t-1}, \theta_{k,t}^m, \mathcal{M}_k)$ , obtained from the BPF; see Equation (16). Here,  $\{\omega_{k,t}^m\}_{m=1}^{N_\theta}$  denote the weights of the  $\theta$ -particles, which should not be confused with  $\{w_{k,t}^i\}_{i=1}^{N_x}$ , the weights of the state particles used in Algorithm 1. As time progresses, particle degeneracy may occur, whereby a few  $\theta$ -particles dominate the weight distribution. To mitigate this, a rejuvenation step is applied, consisting of a resampling phase followed by a move step using a particle marginal Metropolis-Hastings (PMMH) kernel (Andrieu et al., 2010). This move step aims to refresh the diversity of parameter particles by applying a few MCMC iterations to each resampled  $\theta$ -particle. These MCMC transitions are constructed to leave the target posterior distribution  $p(\theta_k|y_{1:t}, \mathcal{M}_k)$  invariant. The combination of the resampling and move steps is referred to as the ‘‘rejuvenation’’ step. In this study, new parameters are proposed from a multivariate Gaussian distribution  $\theta_k^* \sim q(\theta_k^*|\theta_{k,t}^m) := \mathcal{N}(\widehat{\mu}_{k,t}, c\widehat{\Sigma}_{k,t})$ , where  $c$  is a scaling factor. The mean and covariance matrix are given by:

$$\widehat{\mu}_{k,t} = \frac{1}{\sum_{m=1}^{N_\theta} \omega_{k,t}^m} \sum_{m=1}^{N_\theta} \omega_{k,t}^m \theta_{k,t}^m, \quad \text{and} \quad \widehat{\Sigma}_{k,t} = \frac{1}{\sum_{m=1}^{N_\theta} \omega_{k,t}^m} \sum_{m=1}^{N_\theta} \omega_{k,t}^m (\theta_{k,t}^m - \widehat{\mu}_{k,t})(\theta_{k,t}^m - \widehat{\mu}_{k,t})^T, \quad (19)$$

It is worth noting that alternative proposals, such as a random walk proposal applied to the current set of particles, can also be used (Chopin and Papaspiliopoulos, 2020). The resampling in the rejuvenation step is similar to the one used in Algorithm 1 but is performed only when the effective sample size (ESS), which is an assessment of the degeneracy of the parameter particles, falls below a threshold  $\tau_R$ ; in that case a degeneracy criterion is deemed to be met. The ESS for model  $k$  is given by

$$\text{ESS}_k = \left( \sum_{m=1}^{N_\theta} \omega_{k,t}^m \right)^2 / \sum_{m=1}^{N_\theta} (\omega_{k,t}^m)^2. \quad (20)$$

In practice, an ESS threshold of 50% ( $\tau_R = 0.5$ ) is commonly used (Chopin et al., 2013; Chopin and Papaspiliopoulos, 2020). Each rejuvenation step involves computing an unbiased estimate of the marginal likelihood given a proposed parameter  $\theta^*$ , by running Algorithm 1 over observations from time 1 to  $t$ . The proposed parameter is then either accepted or rejected based on the Metropolis-Hastings acceptance probability:

$$\alpha_k = \min \left\{ 1, \frac{\widehat{p}_{N_x}(y_{1:t}|\theta_k^*, \mathcal{M}_k) p(\theta_k^*)}{\widehat{p}_{N_x}(y_{1:t}|\theta_{k,t}^m, \mathcal{M}_k) p(\theta_{k,t}^m)} \times \frac{q(\theta_{k,t}^m|\theta_k^*)}{q(\theta_k^*|\theta_{k,t}^m)} \right\} \quad (21)$$

This procedure enables us to incorporate parameter uncertainty into our model evidence estimation (see Chopin et al. (2013) for technical details). Specifically, the marginal likelihood under model  $\mathcal{M}_k$  is approximated by the product of the weighted averages of the incremental likelihoods:

$$p(y_{1:t}|\theta_k, \mathcal{M}_k) \approx \widehat{Z}_{k,t} = \prod_{s=1}^t \left( \frac{1}{\sum_{m=1}^{N_\theta} \omega_{k,s-1}^m} \sum_{m=1}^{N_\theta} \omega_{k,s-1}^m \widehat{p}_{N_x}(y_s|y_{1:s-1}, \theta_{k,s}^m, \mathcal{M}_k) \right). \quad (22)$$

For many diseases, the dynamics of transmission can change at unknown times, leading to a need for adaptation. For instance, transitions may occur from a pre-epidemic phase to an epidemic phase, or from an epidemic phase to a controlled phase. Each of these phases is characterized by distinct disease dynamics and observable data, making it essential to detect and model these changes effectively. This scenario can be viewed as a change detection problem, where the system must identify shifts in transmission patterns to update the modeling approach accordingly. A simple yet effective method to address the challenges of time-varying models is to utilize a sliding window of  $t_w$  time steps, resetting all model evidence every  $t_w$  iterations (Martino et al. (2015), Section 5). For this approach, the model evidence is approximated through

$$\widehat{Z}_{k,t} = \prod_{s=t-t_w+1}^t \left( \frac{1}{\sum_{m=1}^{N_\theta} \omega_{k,s-1}^m} \sum_{m=1}^{N_\theta} \omega_{k,s-1}^m \widehat{p}_{N_x}(y_s|y_{1:s-1}, \theta_{k,s}^m, \mathcal{M}_k) \right). \quad (23)$$

This approach is particularly useful when the relative performance of the models under consideration changes during the different phases of an outbreak.

Hence, by replacing  $p(y_{1:t}|\theta_k, \mathcal{M}_k)$  in Equation (10) with its SMC<sup>2</sup> approximation, we obtain a sequential estimate of the posterior model probability  $\pi_{k,t}$  is given by:

$$\pi_{k,t} \approx \frac{\widehat{Z}_{k,t}}{\sum_{j=1}^2 \widehat{Z}_{j,t}}, \quad k = 1, 2. \quad (24)$$

We consider two models, but the proposed approach could be adapted to include more than two. The SMC<sup>2</sup> scheme for model averaging incorporating a sliding window is outlined in Algorithm 2. Step 1 simply requires generating the initial parameter particles from a carefully chosen prior distribution. Steps 8–11 are repeated  $M$  times, where  $M$  is the number of PMMH moves.

---

**Algorithm 2** Bayesian model averaging using SMC<sup>2</sup> (BMA-SMC<sup>2</sup>)

Operations involving indexes  $k$  and  $m$  must be performed for  $k = 1, 2$  and  $m = 1, \dots, N_\theta$ . The indices  $a_{1:N_\theta}$  define the ancestral parameter particles after the resampling.

**Inputs:** Observation:  $y_{1:T}$ , Prior:  $p(\theta_k)$ , Inital state distribution:  $f_k(x_{k,0}|\theta_k)$ , Number of state particles:  $N_x$ , Number of parameter particles:  $N_\theta$ , Resample threshold :  $\tau_R$ ,

Number of PMMH Move:  $M$ , Refreshing window:  $t_w$ ,

**Output:** Particle set:  $\{\theta_{k,0:t}^m, x_{k,0:t}^{1:N_x}, \pi_{k,0:t}\}$ .

---

- 1: Sample a initial particles  $\theta_{k,0}^m \sim p(\theta_k)$  and set  $\omega_{k,0}^m = 1/N_\theta$ .
- 2: **for**  $t = 1$  to  $T$  **do**
- 3:     Perform iteration  $t$  of the Algorithm 1 using  $\theta_{k,t}^m$  to obtain  $\{x_{k,t,\theta_{k,t}^m}^{1:N_x}, w_{k,t,\theta_{k,t}^m}^{1:N_x}\}$  and  $\widehat{p}_{N_x}(y_t|y_{1:t-1}, \theta_{k,t}^m, \mathcal{M}_k)$  and compute  $\widehat{p}_{N_x}(y_{1:t}|\theta_{k,t}^m, \mathcal{M}_k)$  using Equation (17)
- 4:     Update importance weights:  $\omega_{k,t}^m = \omega_{k,t-1}^m \widehat{p}_{N_x}(y_t|y_{1:t-1}, \theta_{k,t}^m)$ ,  $\omega_{k,t}^m = \omega_{k,t}^m / \sum_{j=1}^{N_x} \omega_{k,t}^j$
- 5:     **if**  $\text{ESS}_k < \tau_R N_\theta$  **then**
- 6:         Sample new indices  $a_{1:N_\theta} \sim \text{Resample}(\omega_t^{1:N_\theta})$
- 7:         Set  $\{\theta_{k,t}^m, \omega_{k,t}^m\} := \{\theta_{k,t}^{a_m}, 1/N_\theta\}$ ,  $\{x_{k,t,\theta_{k,t}^m}^{1:N_x}, w_{k,t,\theta_{k,t}^m}^{1:N_x}\} := \{x_{k,t,\theta_{k,t}^{a_m}}^{1:N_x}, w_{k,t,\theta_{k,t}^{a_m}}^{1:N_x}\}$
- 8:         Propose  $\theta_k^* \sim q(\theta_k^*|\theta_{k,t}^m)$  run the the Algorithm 1 using  $\theta_k^*$  and observations  $y_{1:t}$  to obtain  $\{x_{k,t,\theta_k^*}^{1:N_x}, w_{k,t,\theta_k^*}^{1:N_x}\}$  and  $\widehat{p}_{N_x}(y_{1:t}|\theta_{k,t}^*, \mathcal{M}_k)$
- 9:         Compute :  $\alpha_k = \min \left\{ 1, \frac{\widehat{p}_{N_x}(y_{1:t}|\theta_k^*, \mathcal{M}_k) p(\theta_k^*)}{\widehat{p}_{N_x}(y_{1:t}|\theta_{k,t}^m, \mathcal{M}_k) p(\theta_{k,t}^m)} \times \frac{q(\theta_{k,t}^m|\theta_k^*)}{q(\theta_k^*|\theta_{k,t}^m)} \right\}$
- 10:         Set  $(\theta_{k,t}^m, x_{k,t,\theta_{k,t}^m}^{1:N_x}, w_{k,t,\theta_{k,t}^m}^{1:N_x}) = \begin{cases} (\theta_k^*, x_{k,t,\theta_k^*}^{1:N_x}, w_{k,t,\theta_k^*}^{1:N_x}) & \text{with probability } \alpha_k \\ (\theta_{k,t}^m, x_{k,t,\theta_{k,t}^m}^{1:N_x}, w_{k,t,\theta_{k,t}^m}^{1:N_x}) & \text{with probability } 1 - \alpha_k \end{cases}$
- 11:     **end if**
- 12:     Compute model evidence  $\widehat{Z}_{k,t}$  and estimate of the model probability  $\pi_{k,t}$  using (23) and (24), respectively.
- 13: **end for**
- 14: Run the BPF using the estimate of  $\theta_k$  and compute the average estimates of interest via:

$$\widehat{\Delta}_t = \text{E}[\Delta_t|y_{1:t}] \approx \sum_{k=1}^2 \pi_{k,t} \left( \frac{1}{N_x} \sum_{i=1}^{N_x} \Delta_{k,t}^i \right)$$

where  $\Delta_t$  is one of  $\lambda(t), R_t$  i.e. a common quantity of interest across the models.

---

Given that both the DTHP and SEIR models provide filtered estimates of the daily incidence and the reproduction number, the model averaged estimates at each time step, denoted as  $\widehat{\lambda}(t)$  for the daily incidence and  $\widehat{R}_t$  for the reproduction number, are calculated as follows:

$$\widehat{\lambda}(t) = \sum_{k=1}^2 \pi_{k,t} \widehat{\lambda}_k(t), \quad \widehat{\lambda}_k(t) = \text{E}[\lambda_k(t)|y_{1:t}] \approx \frac{1}{N_x} \sum_{i=1}^{N_x} \lambda_k^i(t), \quad (25)$$

$$\widehat{R}_t = \sum_{k=1}^2 \pi_{k,t} \widehat{R}_{k,t}, \quad \widehat{R}_{k,t} = \text{E}[R_{k,t}|y_{1:t}] \approx \frac{1}{N_x} \sum_{i=1}^{N_x} R_{k,t}^i, \quad (26)$$

where  $\{\lambda_k^i(t)\}_{i=1}^{N_x}$  and  $\{R_{k,t}^i\}_{i=1}^{N_x}$  represent the particle incidence and the reproduction number, respectively, for the model  $\mathcal{M}_k$  based on data up to time  $t$  and the coefficient  $\pi_{k,t}$  given

in Equation (24). The weights  $w_{k,t}^i$  are particle weights for model  $k$  at time  $t$  obtained by running the BPF using the parameter value  $\theta_k$  sampled from the SMC<sup>2</sup>.

A key advantage of sequential methods lies in their inherently parallel architecture. Most computations such as particle propagation and weight updates may be performed independently across particles. This structure enables efficient parallelization, allowing Algorithm 2 to scale linearly with the number of state particles ( $N_x$ ) and parameter particles ( $N_\theta$ ). This significantly reduces computation time by utilizing all available CPU cores. The algorithm is implemented in Python (version 3.10.12) and was executed on a desktop computer with an Intel Core i7-1300H processor running at 3.40 GHz. The source code is publicly available at <https://github.com/Dhorasso/bma-smc2-dthp-seir>.

## 4 Results

### 4.1 Experimental setup

To assess the effectiveness of model averaging using the BMA-SMC<sup>2</sup> scheme in estimating daily incidence and the time-varying reproduction number, we conducted a simulation study with synthetic data. The experimental study has two objectives: first, to determine whether Model Averaging (MA) outperforms the individual DTHP and SEIR models, and second, to compare the forecasting accuracy of these models under different epidemiological scenarios. Synthetic data were generated using the SEIR model specified in Equation (2), with a mean incubation period of  $1/\sigma = 2$  days and a mean infectious period of  $1/\gamma = 6$  days. The simulation was run over 100 time periods with a population size of  $N = 50000$ . A time series of daily incidence was generated by recording the number of individuals transitioning from the exposed ( $E$ ) to the infectious ( $I$ ) compartment each day. This was based on a predefined trajectory for the transmission rate  $\beta_t$ , designed to reflect various plausible epidemic patterns. The simulated observations  $y_t$ , for  $t = 1, \dots, 86$  represent noisy measurements of daily incidence. Beyond day 86, the models are projected forward for 14 days (2 weeks); the data from  $T = 86$  days onward were excluded from the model-fitting process.

Three distinct epidemiological scenarios with the initial condition  $(S(0), E(0), I(0), R(0)) = (N - 10, 0, 10, 0)$  were developed to test the robustness and adaptability of the models under varied infection dynamics:

- (a) **Scenario A** represents an initial phase of moderate transmission that declines significantly over time. Specifically, for  $t \leq 40$ , the transmission rate is set at  $\beta_t = 0.32$ . This rate then decreases progressively, and for  $45 \leq t \leq 100$ , it is fixed at  $\beta_t = 0.14$ , reflecting the impact of effective and sustained control measures.
- (b) **Scenario B** introduces more complex dynamics, characterized by a high initial transmission rate that sharply decreases, followed by a subsequent rebound before stabilizing. Here, for  $t \leq 45$ ,  $\beta_t = 0.35$ ; for  $45 < t \leq 80$ ,  $\beta_t = 0.1$ ; and for  $80 \leq t \leq 100$ ,  $\beta_t$  increases to 0.22, capturing fluctuating intervention efforts and partial resurgence in transmission.
- (c) **Scenario C** models a highly dynamic setting, where the transmission rate varies nonlinearly as  $\beta_t = 0.28 \exp(\cos(2\pi t/100) - t/128)$ . This captures oscillatory and time-varying transmission patterns, potentially driven by seasonal factors.

### 4.2 Evaluation Metrics

To assess model performance, we employ three key metrics: Root Mean Square Error (RMSE), coverage of predictive credible intervals ( $\text{Coverage}_\alpha$ ), and the Continuous Ranked Probability Score (CRPS).

RMSE quantifies the average deviation between the model’s predicted mean and the observed data. It is defined as:

$$\text{RMSE} = \sqrt{\frac{1}{T} \sum_{t=1}^T (z_t - \widehat{\Delta}_t)^2}$$

where  $z_t$  is the true value of the incidence (respectively reproduction number) at time  $t$ , and  $\widehat{\Delta}_t = E[\Delta_t | y_{1:t}]$  is the model posterior predictive mean of the incidence (respectively reproduction number) at time  $t$  as define in Equations (25) and (26).

Coverage $_{\alpha}$  allows to assess the calibration of the model’s uncertainty estimates by measuring the proportion of true observations that fall within the  $(1 - \alpha) \times 100\%$  credible interval. In our case, we use  $\alpha = 0.05$ , corresponding to the 95% credible interval:

$$\text{Coverage}_{\alpha} = \frac{1}{T} \sum_{t=1}^T \mathbb{I}(z_t \in \text{CI}_{\alpha,t})$$

where  $\mathbb{I}(\cdot)$  is the indicator function, and  $\text{CI}_{\alpha,t}$  denotes the  $(1 - \alpha)$ -level credible interval of the predictive distribution at time  $t$ .

CRPS evaluates the quality of the full predictive distribution by comparing the model-predicted cumulative distribution function (CDF) to the empirical CDF of the observation. It is defined as:

$$\text{CRPS} = \frac{1}{T} \sum_{t=1}^T \int_{-\infty}^{\infty} (F_t(u) - \mathbb{I}(z_t \leq u))^2 du$$

where  $F_t(u) = p(\Delta_t \leq u | y_{1:T})$  is the predictive CDF at time  $t$ . Lower CRPS values indicate more accurate and sharper probabilistic prediction. When the predictive distribution is represented by a set of particles  $\{\Delta_t^i\}_{i=1}^{N_x}$ , CRPS can be approximated as:

$$\text{CRPS} \approx \frac{1}{T} \sum_{t=1}^T \left( \frac{1}{N_x} \sum_{i=1}^{N_x} |z_t - \Delta_t^i| - \frac{1}{2N_x^2} \sum_{i=1}^{N_x} \sum_{j=1}^{N_x} |\Delta_t^i - \Delta_t^j| \right)$$

This formulation captures both the bias and the dispersion of the predictive distribution (Jordan et al., 2019).

For the DTHP model, we assume that all new cases arise from transmission by existing infected individuals within the population, with no contribution from imported or spontaneous cases (i.e.,  $\mu = 0$  in Equation (1)). Table B.1 in the supplementary material provides the prior distribution used to sample the initial state and parameter particles for each model across all scenarios. For each model, Algorithm 2 was executed with:  $N_{\theta} = 400$  parameter particles and  $N_x = 200$  state particles, with  $M = 5$  successive PMMH moves. We employed a sliding window of one time step ( $t_w = 1$ ) for computing the model evidence (see Equation (23)), which means the models are weighted based on the one-step-ahead predictive likelihood (Parrish et al., 2012; Martino et al., 2015). This choice was motivated by simulated results (not shown here) that indicated a one-step window provides slightly better predictions for model averaging in scenarios with rapidly changing dynamics, compared to using the full model evidence as described in Equation (22).

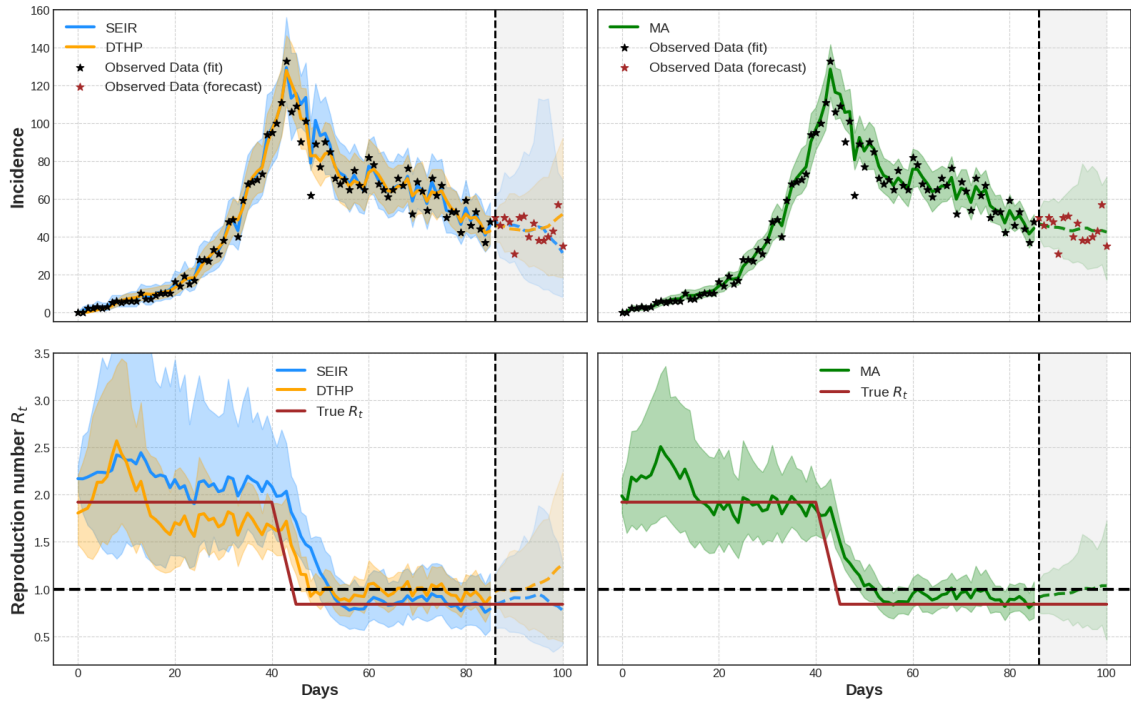


Figure 1: **Simulated daily incidence and time-varying reproduction number for Scenario A.** The black/brown stars correspond to the observed incidence data, and the true underlying  $R_t$  is shown as a solid brown line. The solid lines represent the posterior mean estimates of the incidence and  $R_t$  obtained from the DTHP (orange), SEIR (blue), and MA (green) approaches, with shaded areas indicating the associated 95% credible intervals. The vertical black dashed line marks the start of the forecasting period.

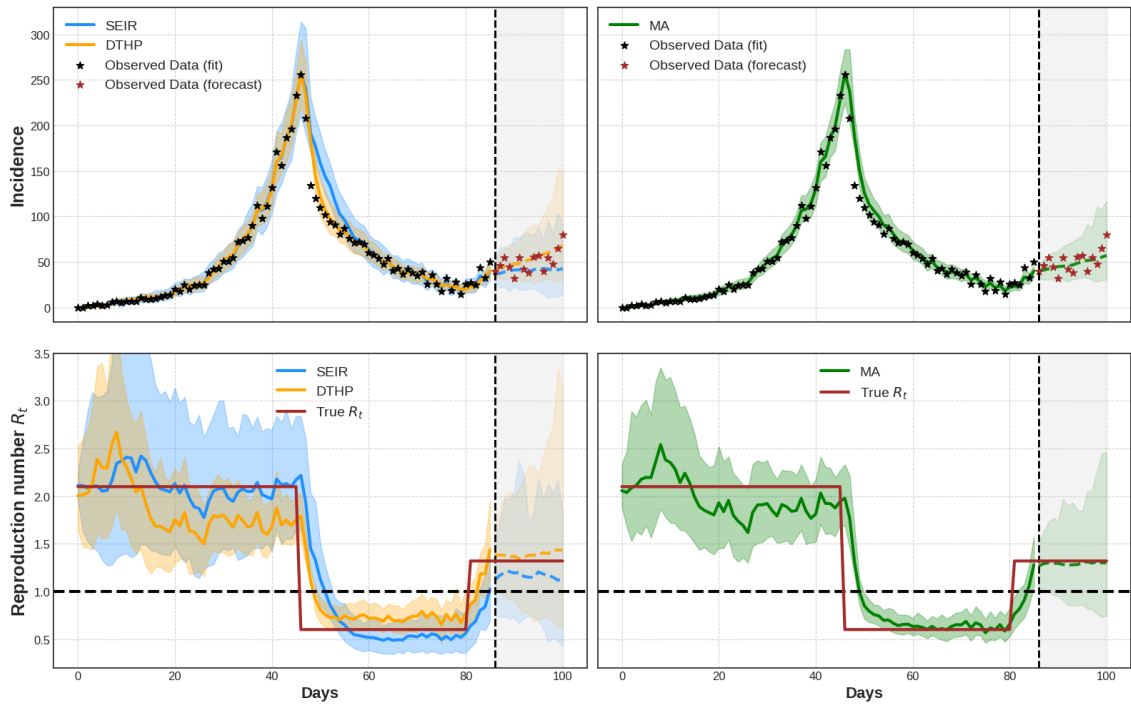


Figure 2: **Simulated daily incidence and time-varying reproduction number for Scenario B.** The black/brown stars correspond to the observed incidence data, and the true underlying  $R_t$  is shown as a solid brown line. The solid lines represent the posterior mean estimates of the incidence and  $R_t$  obtained from the DTHP (orange), SEIR (blue), and MA (green) approaches, with shaded areas indicating the associated 95% credible intervals. The vertical black dashed line marks the start of the forecasting period.

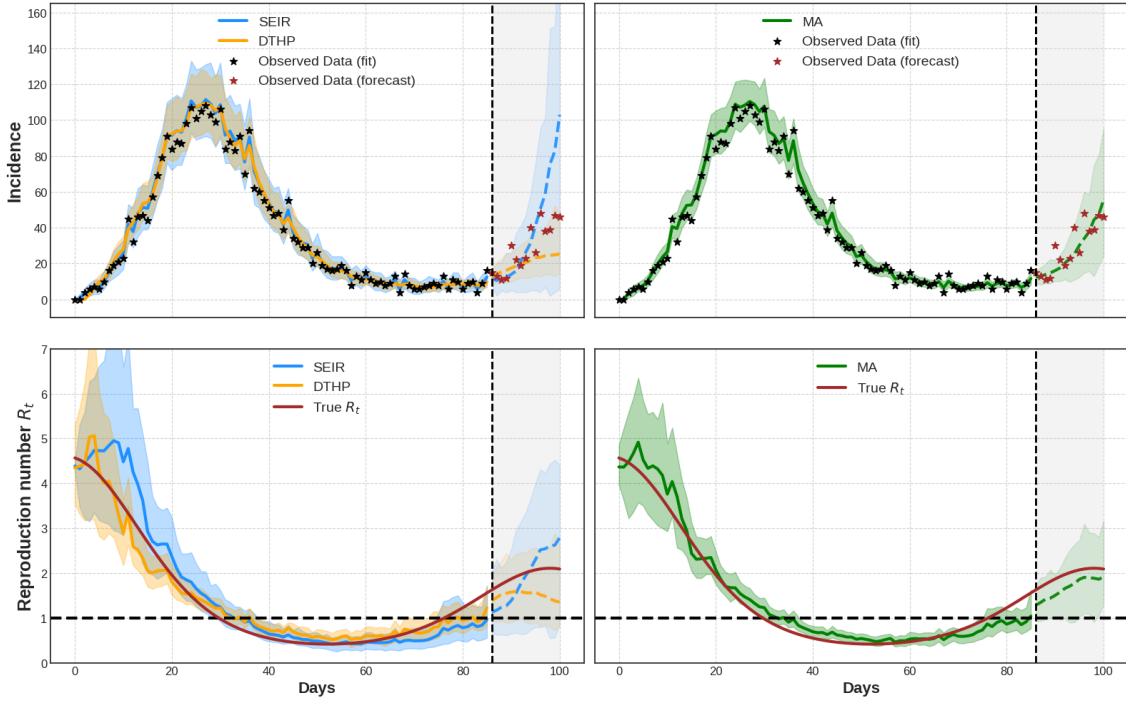


Figure 3: **Simulated daily incidence and time-varying reproduction number for Scenario C.** The black/brown stars correspond to the observed incidence data, and the true underlying  $R_t$  is shown as a solid brown line. The solid lines represent the posterior mean estimates of the incidence and  $R_t$  obtained from the DTHP (orange), SEIR (blue), and MA (green) approaches, with shaded areas indicating the associated 95% credible intervals. The vertical black dashed line marks the start of the forecasting period.

In Figures 1–3, the three approaches (DTHP, SEIR, and MA) were evaluated across different scenarios (A, B, and C), showing how well they estimate daily incidence and track the time-varying reproduction number. The shaded areas represent 95% credible intervals that show uncertainty. Performance is also summarized using within-sample and forecast metrics in Tables 1 and 2.

In Scenario A (Figure 1), which represents a controlled epidemic with gradually declining transmission, all models provide close fits to the observed incidence data during the training period. The MA exhibits notably smooth estimates and comparatively narrow credible intervals. Its estimates of  $R_t$  reflect a clearer downward trend, with reduced uncertainty. As seen in Table 1, MA achieves the lowest RMSE and CRPS for both incidence and  $R_t$  during the fitting period. Forecast performance remains strong for all the models, with MA offering tighter and more concentrated forecast intervals for incidence, as reflected in Table 2. For  $R_t$ , all models achieve full forecast coverage, but SEIR attains the most precise point forecasts.

In Scenario B (Figure 2), which introduces abrupt changes in transmission dynamics, more pronounced differences emerge across models. During the training period, MA and DTHP more accurately track the observed incidence compared to SEIR, which fails to capture the sudden decrease in the incidence after day 45. MA also provides more stable estimates of  $R_t$  with less temporal variability. The MA yields the lowest CRPS for both incidence and  $R_t$ , and competitive RMSE (Table 1). In forecasting incidence, MA outperforms both competing models with lower errors and well-calibrated predictive intervals, whereas SEIR’s forecasts are less reliable despite moderate accuracy. DTHP provides good coverage but suffers from higher forecast errors, especially in the projection of incidence trends, reflecting difficulty in anticipating complex future dynamics under this scenario. For  $R_t$ , all models maintain perfect forecast coverage, with MA again achieving the best balance of accuracy and sharpness (Table 2).

Scenario C (Figure 3) features rapid and oscillatory changes in transmission, leading to more nuanced model performance. During training, SEIR achieves an excellent fit for

incidence, while the MA model remains competitive with stable  $R_t$  estimates. In forecasting, MA consistently produces sharper and better-calibrated projections, particularly for incidence. SEIR provides strong coverage but with wider predictive uncertainty, whereas DTHP tends to slightly underestimate future cases. For  $R_t$ , all models maintain forecast coverage, with MA generally delivering the most balanced performance (Table 2).

Table 1: Summary of within-sample model performance across Scenarios A, B, and C.

Variable	Metric	Scenario A			Scenario B			Scenario C		
		DTHP	SEIR	MA	DTHP	SEIR	MA	DTHP	SEIR	MA
Incidence	RMSE	4.784	4.587	<b>4.166</b>	<b>6.766</b>	12.656	8.161	4.224	<b>3.167</b>	3.539
	Coverage $_{\alpha}$	0.942	0.965	<b>0.977</b>	0.872	0.919	<b>0.942</b>	0.837	<b>1.00</b>	0.907
	CRPS	2.426	2.270	<b>2.001</b>	3.001	4.459	<b>2.952</b>	2.320	<b>1.704</b>	1.801
$R_t$	RMSE	0.226	0.291	<b>0.219</b>	0.330	0.338	<b>0.297</b>	0.257	0.422	<b>0.250</b>
	Coverage $_{\alpha}$	0.802	<b>0.884</b>	0.837	0.628	<b>0.872</b>	0.860	0.651	<b>0.907</b>	0.640
	CRPS	0.131	0.145	<b>0.113</b>	0.203	0.167	<b>0.146</b>	0.153	0.198	<b>0.142</b>

The results demonstrate that MA delivers consistent advantages across a variety of epidemic conditions, especially in capturing underlying trends and maintaining well-balanced forecast uncertainty. While individual models may perform well under specific circumstances, MA generally provides the most stable and reliable performance by integrating their complementary strengths. Notably, even in cases where MA is not the top-performing model, it remains closely competitive, typically ranking second across both within-sample and forecast metrics (Tables 1 and 2). Furthermore, the BMA-SMC<sup>2</sup> framework enables dynamic tracking of model parameter distributions over time ( $t = 1, \dots, T$ ), allowing for real-time assessment of parameter uncertainty, as illustrated in Figures B.2-B.4 of the supplementary material.

Table 2: Summary of out-of-sample model performance across Scenarios A, B, and C.

Variable	Metric	Scenario A			Scenario B			Scenario C		
		DTHP	SEIR	MA	DTHP	SEIR	MA	DTHP	SEIR	MA
Incidence	RMSE	7.361	7.971	<b>6.763</b>	13.036	11.739	<b>9.235</b>	12.848	21.430	<b>7.231</b>
	Coverage $_{\alpha}$	<b>1.00</b>	<b>1.00</b>	0.933	<b>1.00</b>	0.933	<b>1.00</b>	0.800	<b>0.933</b>	<b>0.933</b>
	CRPS	4.274	5.569	<b>3.960</b>	6.592	8.354	<b>5.722</b>	7.792	9.845	<b>4.054</b>
$R_t$	RMSE	0.235	<b>0.060</b>	0.141	0.141	0.250	<b>0.055</b>	0.483	0.440	<b>0.290</b>
	Coverage $_{\alpha}$	<b>1.00</b>	<b>1.00</b>	<b>1.00</b>	<b>1.00</b>	<b>1.00</b>	<b>1.00</b>	<b>1.00</b>	<b>1.00</b>	<b>1.00</b>
	CRPS	0.126	<b>0.066</b>	0.075	0.097	0.173	<b>0.079</b>	0.310	0.309	<b>0.189</b>

### 4.3 Analysis of real data: Irish Influenza and COVID-19 epidemics

We applied our methodology to real-world data from Ireland, using weekly influenza cases and daily COVID-19 case counts. The data were obtained from the Health Protection Surveillance Centre (HPSC)<sup>12</sup>.

For influenza, we analyzed weekly cases from May 29, 2022, to June 16, 2024, a period after most COVID-19 restrictions had ended. This allowed for a clear assessment of post-pandemic influenza dynamics. Inference was performed using methods described in Section 2 using instead a SEIRS model; see Section C of the supplementary material for details. Historical data from the first 94 weeks was used for sequential training and then to generate 14-week-ahead forecasts. Forecasts were obtained by propagating the inferred latent states forward in time under the state-space model dynamics.

<sup>1</sup><https://respiratorydisease-hpscireland.hub.arcgis.com/pages/influenza>

<sup>2</sup><https://COVID19ireland-geohive.hub.arcgis.com/>

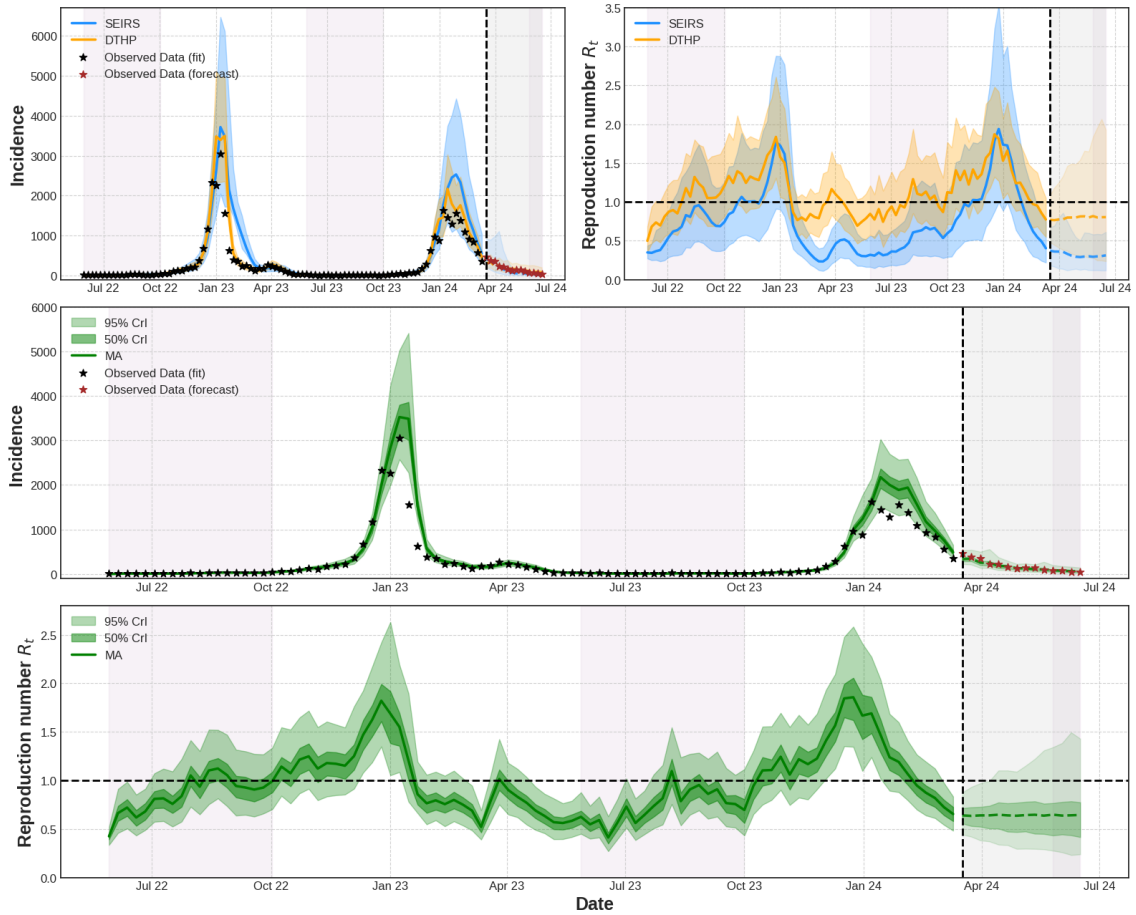


Figure 4: **Weekly incidence data from the Influenza pandemic and corresponding filtering estimate of the time-varying reproduction number for the DTHP and SEIRS models.** The black/brown stars correspond to the observed data for incidence. The solid lines represent the posterior mean estimates of the incidence and  $R_t$  obtained from the DTHP (orange), and SEIRS (blue) approaches, with shaded areas indicating the associated 95% credible intervals. The vertical black dashed line marks the start of the forecasting period, and the light gray area highlights the forecast window. Summer periods are indicated by a light pink area.

In Figure 4, we present model predictions of influenza incidence and the corresponding  $R_t$  estimates, highlighting the comparative strengths of the SEIRS, DTHP, and MA. The SEIRS model provides robust coverage but fails to capture the sharp decline in cases during the first wave and overestimates the peak in the second wave. In contrast, the DTHP model closely tracks the changes in observed cases, but it underperforms during forecasting. Both models yield similar  $R_t$  trends, with slight differences in magnitude during the period of low incidence between the peaks. The MA combines the strengths of both approaches, capturing abrupt changes like the DTHP while preserving the broader structure of the SEIRS model. It achieves the best overall performance, with the lowest in-sample RMSE, and maintains accuracy and calibration during forecasts from March 10 to June 16, 2024, outperforming both baselines in RMSE, coverage and CRPS (Table 3). Its uncertainty bounds are narrower than those of the SEIRS model, and its predictions closely follow the observed data. The  $R_t$  estimates capture seasonal variations, with transmission peaking during winter months: in 2022–2023, dominated by Influenza A (Health Protection Surveillance Centre, 2024),  $R_t$  peaked at 1.82 (95% CI: 1.35–2.42), and in 2023–2024, it reached 1.85 (95% CI: 1.34–2.58) before declining significantly by June 30, 2024.

Table 3: Summary of model performance on Influenza and COVID-19 data.

Disease	Metric	In-Sample			Projection		
		DTHP	SEIRS	MA	DTHP	SEIRS	MA
Influenza	RMSE	285.672	404.850	<b>277.412</b>	63.988	54.748	<b>47.946</b>
	Coverage $_{\alpha}$	0.798	<b>0.872</b>	<b>0.872</b>	0.929	0.643	<b>1.00</b>
	CRPS	<b>70.260</b>	123.415	71.684	32.593	56.148	<b>25.073</b>
COVID-19	RMSE	87.261	87.415	<b>86.790</b>	75.374	<b>73.786</b>	74.473
	Coverage $_{\alpha}$	0.688	0.804	0.591	<b>0.929</b>	<b>0.929</b>	0.857
	CRPS	38.266	<b>35.978</b>	38.803	42.790	47.155	<b>42.585</b>

Note: For Influenza, the SEIRS model was used in place of the SEIR model.

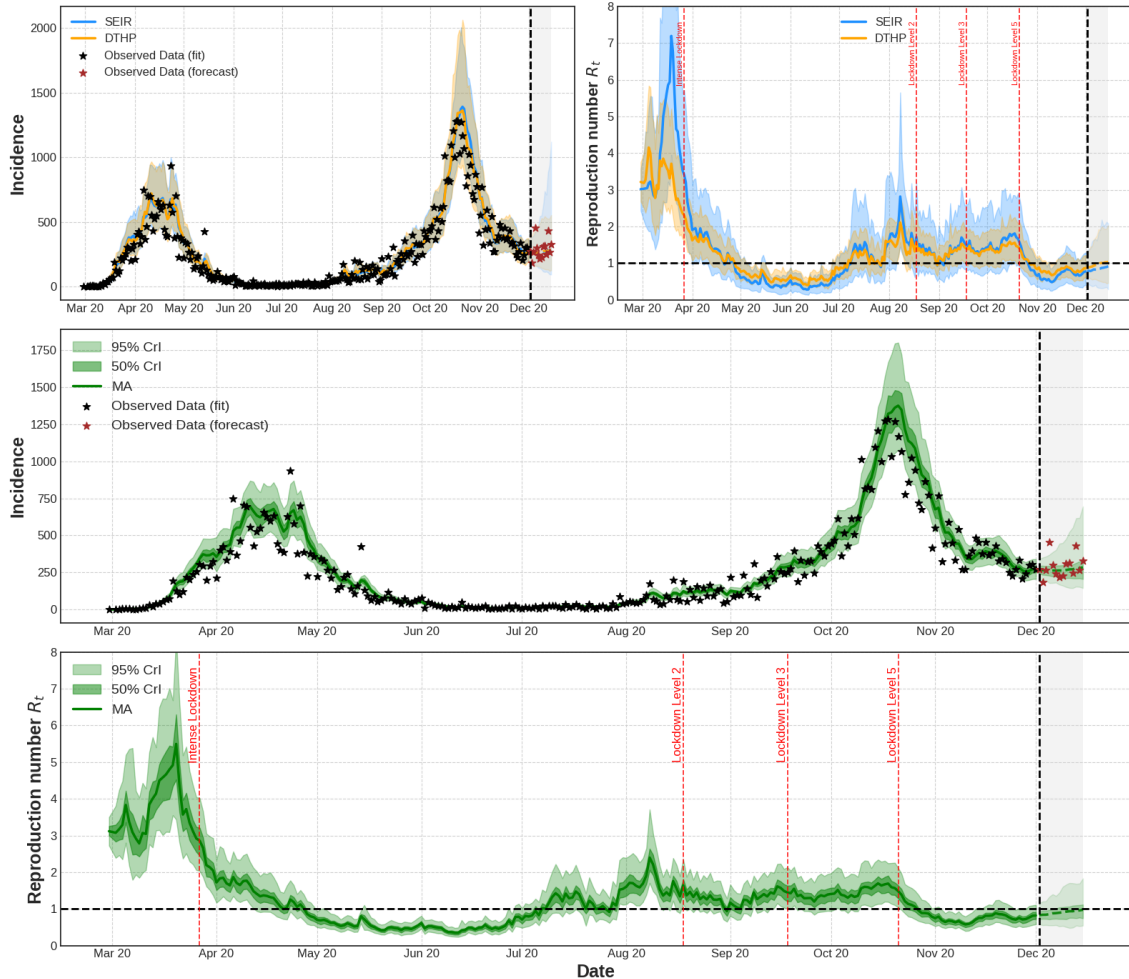


Figure 5: Daily case incidence from the COVID-19 and corresponding filtering estimate of the time-varying reproduction number. The black/brown stars correspond to the observed data for incidence. The solid lines represent the posterior mean estimates of the incidence and  $R_t$  obtained from the DTHP (orange), SEIR (blue), and MA (green) approaches, with shaded areas indicating the associated 95% credible intervals. Vertical red dashed lines mark the start dates of major mitigation measures, the vertical black dashed line indicates the beginning of the forecasting period, and the light gray area denotes the forecast window.

For COVID-19, we focused on the initial waves from February 29 to December 15, 2020, a period marked by high transmission and changing interventions. Here, we use DTHP and SEIR models. Figure 5 shows that all models closely fit the observed incidence, successfully capturing the two epidemic waves, with the MA model producing narrower uncertainty bands during the peak of the second wave. The 2-week forecasts from December 1 also align well with the actual observations. Both SEIR and DTHP models show similar  $R_t$  trends, although the SEIR model slightly overestimates early transmission and

yields wider uncertainty bands throughout the study period. The  $R_t$  estimates reflect key dynamics, including a sharp decline following the first lockdown (March 27, 2020), which drove  $R_t$  below one and ended the first wave. As restrictions eased in June,  $R_t$  gradually increased and remained above one until mid-October, marking the start of the second wave. Lockdowns reintroduced in late October brought  $R_t$  below one again by November. Lockdown measures are described in (Jaouimaa et al., 2021). Our  $R_t$  estimates align with previous findings reported in (Jaouimaa et al., 2021; Cazelles et al., 2021).

## 5 Discussion

Dynamic models are essential tools for monitoring disease progression and anticipating new epidemic waves. In this study, we introduced a novel approach to enhance epidemic modeling by combining the strengths of the DTHP and SEIR(S) models through a model-averaging (MA) technique. Our method uses the SMC<sup>2</sup> framework to dynamically integrate predictions from multiple models, yielding a single, robust estimate of shared latent variables while simultaneously estimating static parameters.

Our results demonstrate that both the DTHP and SEIR(S) models are individually able to capture epidemic trends and estimate the time-varying reproduction number,  $R_t$ , under diverse conditions. The DTHP model, which captures self-exciting behavior, performed well during phases marked by abrupt transmission changes. However, it produced less accurate estimates of  $R_t$ , likely due to the limitations of its simplified triggering kernel. In contrast, the SEIR(S) model more accurately represented the overall epidemic trajectory and the evolution of  $R_t$ , but struggled to capture sudden changes in incidence. Additionally, it produced wider credible intervals, possibly reflecting uncertainty in the infectious period, which directly influences  $R_t$  estimates. These observations underscore the limitations of relying on a single model, particularly in complex and rapidly evolving epidemic contexts.

The proposed model-averaging framework balances the complementary strengths of the DTHP and SEIR(S) models, producing well-calibrated forecasts with appropriate uncertainty coverage. It performs robustly in both in-sample and out-of-sample settings, consistently yielding the lowest or near-lowest prediction errors for incidence and  $R_t$  across various simulation scenarios. It also reduces prediction uncertainty, producing narrower credible intervals while maintaining high predictive accuracy. We further demonstrated the practical utility of this framework using empirical data from influenza and COVID-19 outbreaks in Ireland. During the Influenza waves, which featured abrupt changes in transmission, the MA approach successfully combined the benefits of DTHP and SEIR(S), delivering accurate forecasts and reliable estimates. For COVID-19, although improvements were more modest, model averaging yielded more stable  $R_t$  estimates during the early phase of the outbreak and handled uncertainty more effectively. These findings suggest that our sequential model-averaging strategy is a promising approach for real-time epidemic surveillance and forecasting, offering a valuable balance between predictive performance and uncertainty quantification. The sequential ensemble framework further enhances flexibility by continuously updating posterior model probabilities, allowing adaptation to shifting epidemic dynamics (see Figures B.1 and C.2 in the supplementary material). This adaptability is particularly valuable in the where distinct phases of the epidemic may favor different modeling approaches. Note that this comparison focuses on epidemiological modeling using case incidence data and should not be interpreted as a general assessment of the overall performance of individual models.

While model averaging enhances predictive accuracy and robustness, it also introduces challenges. One is interpretability: the combined model’s behavior is often harder to explain than that of its individual components, complicating communication with public health stakeholders. Still, interpretability is partly retained through outputs such as SEIR-derived estimates of latency and infectious periods, or DTHP-triggering kernels that quantify how past infection events influence the expected case counts on any given day

(Browning et al., 2021). These elements provide valuable mechanistic insights into the epidemic process (see Figures B.2–C.2). Another issue is that the combined model may inherit weaknesses from its components, especially if underperforming models keep substantial weight during key periods. Although the SMC<sup>2</sup> weighting scheme adjusts to model fit, it may not fully prevent performance drops when all models perform poorly. Addressing these limitations may require more refined diagnostics of model contributions and adaptive weighting strategies that penalize persistent underperformance. Parameter estimation in each model was carried out using SMC<sup>2</sup>, a method that may suffer from particle degeneracy when abrupt changes occur in the system (see SEIRS parameters in Figure C.1). Extensions to SMC proposed by Birrell et al. (2020) developed to handle what they term “system shocks”, could offer a path forward by improving particle diversity in such scenarios.

Our study assumes all cases result from local transmission and are accurately reported. However, real outbreaks often involve complexities like external infections, under-reporting and reporting delays. Future work could refine the methodology to account for these factors, which would likely improve both the accuracy and applicability. Another promising direction is enhancing the DTHP model with more flexible triggering kernels. Current parametric kernels may miss complex patterns; using Bayesian splines for kernel parametrization would enable a more adaptable, data-driven fit, improving inference.

In summary, our model-averaging framework effectively harnesses the complementary strengths of DTHP and SEIR(S) models to enhance the accuracy and reliability of epidemic forecasts. This method provides a practical tool for real-time epidemic surveillance, with future work aimed at overcoming current limitations and broadening its application to diverse epidemic settings.

## Acknowledgements

This publication has emanated from research conducted with the financial support of Taighde Éireann – Research Ireland under Grant number 21/FFP-P/10123.

## A State forecasting

Once we obtain the filtering estimate of the state vector up to the final time point  $T$  under model  $\mathcal{M}_k$ , using the posterior density  $p(x_{k,T} | y_{1:T}, \theta_k, \mathcal{M}_k)$  for  $k = 1, 2$ , we can use a standard particle filter to compute the  $l$ -step ahead predictive density for  $1 \leq l \leq L$ , denoted by  $p(x_{k,T+l} | y_{1:T}, \theta_k, \mathcal{M}_k)$ . These predicted states are generated by propagating the state model forward without incorporating new observations. A straightforward approach is to sample from the transition distribution  $p(x_{k,T+l} | x_{k,T+l-1}, \theta_k, \mathcal{M}_k)$ . This forecasting procedure is detailed in Algorithm A3. It is important to note that the parameter value  $\theta_k$  used here corresponds to the estimate obtained at time  $T$  from the SMC<sup>2</sup> algorithm.

We assume that the model posterior probabilities for the forecasting period remain the same after the last observation i.e.:  $\pi_{k,T+l} = \pi_{k,T}$ , for  $l = 1, \dots, L$ .

Therefore, the averaged  $L$ -step prediction density of the latent state of interest  $\Delta_{T+l}$  for  $l = 1, \dots, L$  across models can be written as a mixture density:

$$p(\Delta_{T+l} | y_{1:T}) = \pi_{1,T+l} p(\Delta_{T+l} | \theta_1, y_{1:T}, \mathcal{M}_1) + \pi_{2,T+l} p(\Delta_{T+l} | \theta_2, y_{1:T}, \mathcal{M}_2). \quad (27)$$

From this empirical distribution, we can compute the filtered estimate of the latent state  $\Delta_{T+l}$ , for  $l = 1, \dots, L$  as:

$$\widehat{\Delta}_{T+l} = E[\Delta_t | y_{1:T}] \approx \sum_{k=1}^2 \pi_{k,T+l} \left( \sum_{i=1}^{N_x} W_{k,T}^i \Delta_{k,T+l}^i \right), \quad (28)$$

where  $W_{k,T}^i$ ,  $i = 1, \dots, N_x$  are the normalized weights obtained at time  $T$ .

---

**Algorithm A3** State Forecasting in the model  $\mathcal{M}_k$ 

---

- 1: **for**  $l = 1$  to  $L$  **do**
  - 2:     **for**  $i = 1$  to  $N_x$  **do**
  - 3:         Sample a particle :  $x_{k,T+l}^i \sim p(x_{k,T+l}^i | x_{k,T+l-1}^i, \theta_k, \mathcal{M}_k)$
  - 4:         Set:  $x_{k,T:T+l}^i := (x_{k,T:T+l-1}^i, x_{k,T+l}^i)$
  - 5:     **end for**
  - 6:     Compute the  $l$ -step prediction:  $\hat{p}_{N_x}(x_{T+l} | y_{1:T}, \theta_k, \mathcal{M}_k) = \sum_{i=1}^{N_x} W_{k,T}^i \delta_{x_{k,T+l}^i}(x_{T+l})$ .
  - 7: **end for**
- 

## B Parameter distribution in simulated data

Table B.1: Priors used by the models in the simulation scenarios.  $\mathcal{TN}_{[\text{inf}, \text{sup}]}$ (mean,  $\text{std}^2$ ) indicates a truncated normal distribution,  $\mathcal{N}$ (mean,  $\text{std}^2$ ) indicates a normal distribution, and  $\mathcal{U}(\text{inf}, \text{sup})$  indicates a uniform distribution.

Parameter	Model	Scenario A	Scenario B	Scenario C
$\omega$	DTHP	$\mathcal{TN}_{[0, 1]}(0.16, 0.05^2)$		
$R_0$	DTHP	$\mathcal{N}(1.8, 0.05^2)$	$\mathcal{N}(2, 0.05^2)$	$\mathcal{N}(4.25, 0.05^2)$
$\lambda_H(0)$	DTHP	$\mathcal{U}(\{0, \dots, 3\})$		
$\sigma$	SEIR	$\mathcal{TN}_{[0.2, 0.7]}(0.5, 0.05^2)$		
$\gamma$	SEIR	$\mathcal{TN}_{[0, 1]}(0.16, 0.05^2)$	$\mathcal{TN}_{[0, 0.2]}(0.16, 0.1^2)$	
$\beta_0$	SEIR	$\mathcal{N}(0.32, 0.01^2)$	$\mathcal{N}(0.33, 0.01^2)$	$\mathcal{N}(0.725, 0.01^2)$
$(S(0), E(0), I(0), R(0))$	SEIR	$(N - E_0 - I_0, E_0, I_0, 0)$ , with $E_0 \sim \mathcal{U}(\{0, \dots, 5\})$ , $I_0 \sim \mathcal{U}(\{0, \dots, 15\})$ , and $N = 50000$		
$\nu_k, k = 1, 2$	DTHP, SEIR	$\mathcal{TN}_{[0.05, 0.2]}(0.1, 0.01^2)$		
$\phi_k, k = 1, 2$	DTHP, SEIR	$\mathcal{U}([0, 0.1])$		

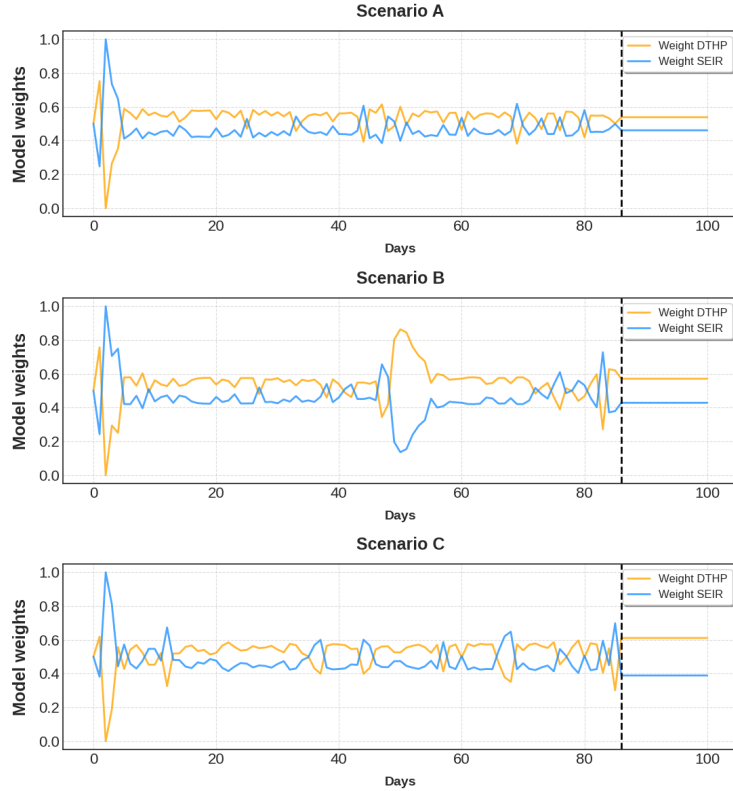


Figure B.1: **Evolution of model weights across scenarios A, B, and C.** The plot illustrates the evolution of model weights of the DTHP and the SEIR model. The vertical black dashed line indicates the start of the forecasting period.

Preliminary experiments suggest that the model is generally not highly sensitive to most parameter settings, with the exception of  $\gamma$  in the SEIR model, which is strongly correlated with the transmission rate  $\beta_t$ . This correlation is especially prominent during abrupt changes in transmission dynamics. The priors on  $\beta_0$  and  $R_0$  are guided by the values used to generate the data for the different scenarios. The prior for  $\nu_k$  allows for rapid changes in the transmission rate, ensuring the model adapts effectively to sudden shifts in disease dynamics, where higher values of  $\nu_k$  correspond to larger changes in the transmission rate.

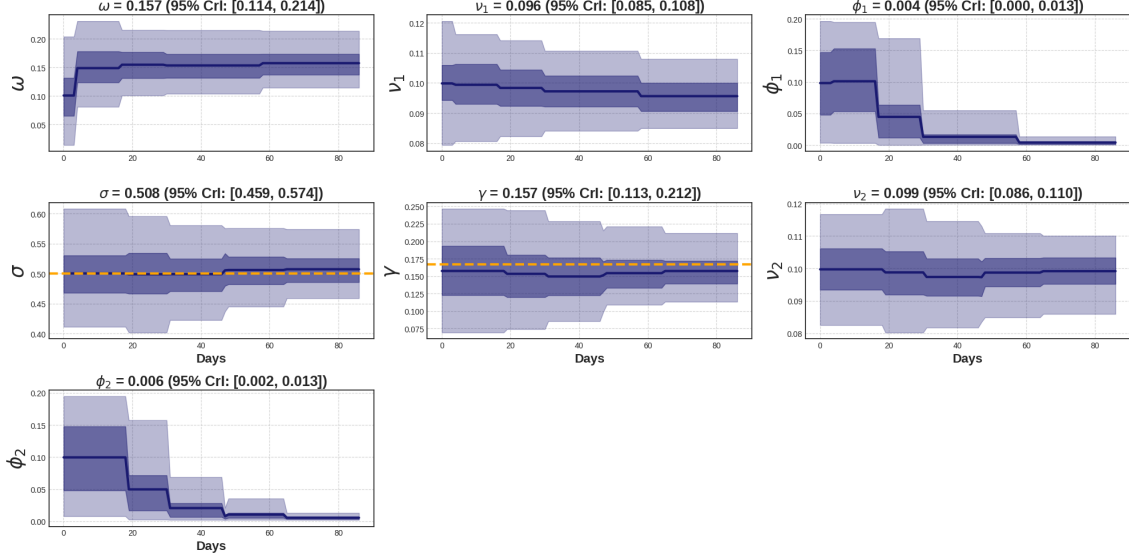


Figure B.2: Evolution of the posterior distributions of each parameter for the DTHP and SEIR models under Scenario A. Posterior means are shown as dark violet lines, with the darker and lighter violet areas indicating the 50% and 95% credible intervals, respectively. The true value of  $\sigma$  and  $\gamma$  used to generate the data is indicated by the horizontal orange dashed line.

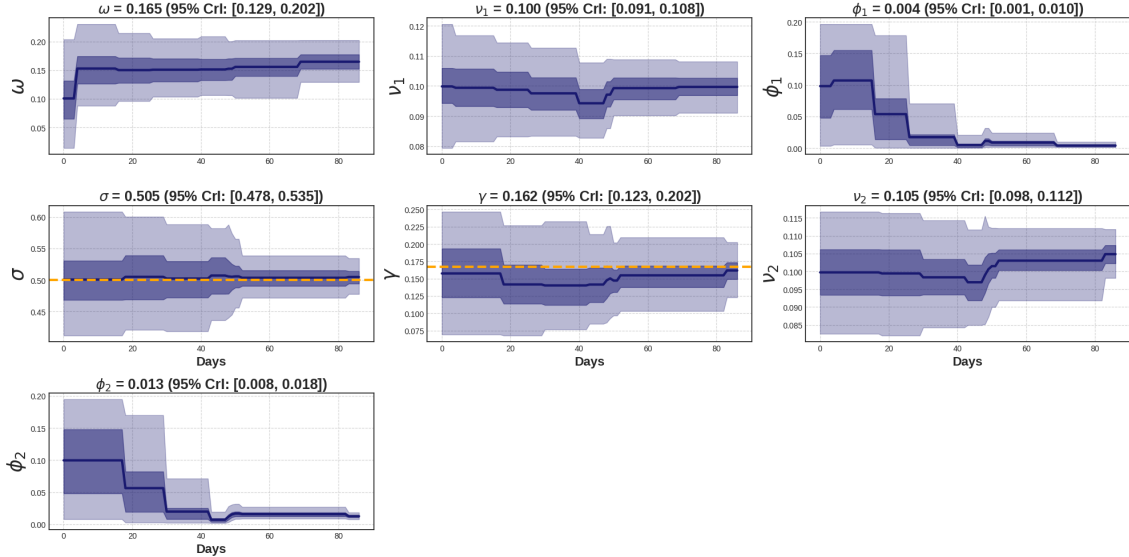


Figure B.3: Evolution of the posterior distributions of each parameter for the DTHP and SEIR models under Scenario B. Posterior means are shown as dark violet lines, with the darker and lighter violet areas indicating the 50% and 95% credible intervals, respectively. The true value of  $\sigma$  and  $\gamma$  used to generate the data is indicated by the horizontal orange dashed line.

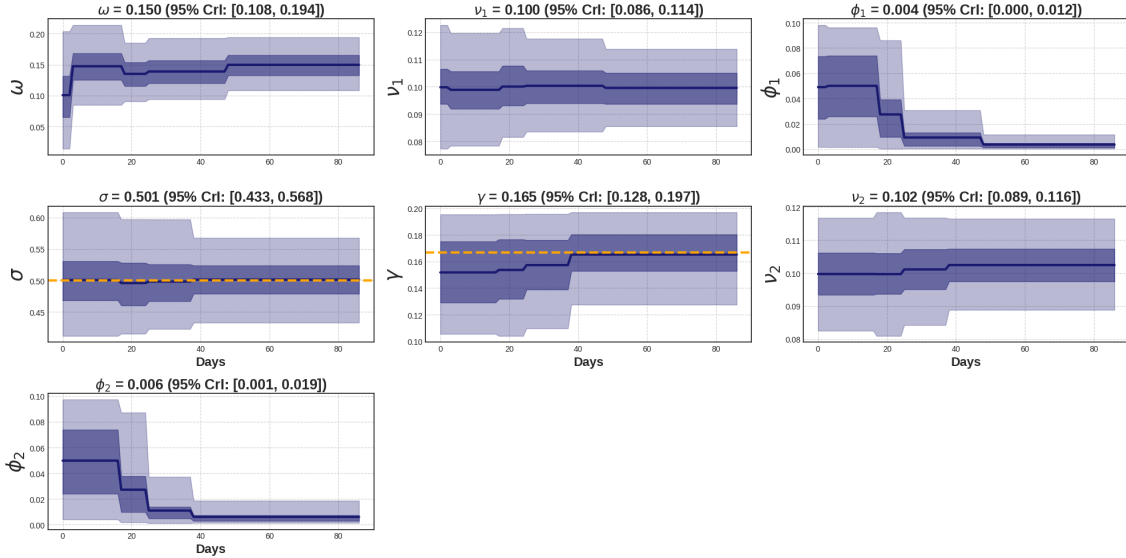


Figure B.4: Evolution of the posterior distributions of each parameter for the DTHP and SEIR models under Scenario C. Posterior means are shown as dark violet lines, with the darker and lighter violet areas indicating the 50% and 95% credible intervals, respectively. The true value of  $\sigma$  and  $\gamma$  used to generate the data is indicated by the horizontal orange dashed line.

## C SEIRS model Influenza and Prior distributions

Given that the dataset spans a period of approximately two years, it is essential to incorporate demographic factors into our model and consider immunity loss. To account for these dynamics, we consider the following SEIRS model:

$$\begin{aligned}
 S(t+1) &= S(t) + \mu(N(t) - S(t)) - \lambda_{SE}(t) + \lambda_{RS}(t), \\
 E(t+1) &= E(t) + \lambda_{SE}(t) - \lambda_{EI}(t) - \mu E(t), \\
 I(t+1) &= I(t) + \lambda_{EI}(t) - \lambda_{IR}(t) - \mu I(t), \\
 R(t+1) &= R(t) + \lambda_{IR}(t) - \mu R(t) - \lambda_{RS}(t).
 \end{aligned} \tag{29}$$

Here, the transitions between compartments are modeled as:

$$\begin{aligned}
 \lambda_{SE}(t) &\sim \text{Binomial}\left(S(t), 1 - e^{-\beta_t \frac{I(t)}{N(t)}}\right), \quad \lambda_{EI}(t) \sim \text{Binomial}(E(t), 1 - e^{-\sigma}), \\
 \lambda_{IR}(t) &\sim \text{Binomial}(I(t), 1 - e^{-\gamma}), \quad \lambda_{RS}(t) \sim \text{Binomial}(R(t), 1 - e^{-\alpha}).
 \end{aligned} \tag{30}$$

The transmission rate  $\beta_t$  as described in the main manuscript. The parameter  $1/\alpha$  denotes the average duration of immunity, while  $1/\sigma$  and  $1/\gamma$  represent the average durations of the latent and infectious periods, respectively. The parameter  $\mu$  denotes the recruitment or mortality rate.

For the SEIRS model, the initial state was set as  $S(0) = N - E(0) - I(0)$ , with  $E(0) \sim \mathcal{U}(\{0, \dots, 5\})$ ,  $I(0) \sim \mathcal{U}(\{0, \dots, 15\})$  and  $R(0) = 0$ , where the total initial population was fixed at  $N = 5.16 \times 10^6$ . The prior distributions for the parameters were specified as follows:  $\mu = 1/(80 \times 52) \text{ weeks}^{-1}$ ,  $\sigma \sim \mathcal{TN}_{[\tau/3, \tau]}(7/1.5, 0.1^2)$ ,  $\gamma \sim \mathcal{TN}_{[1, \tau/5]}(7/6, 0.1^2)$ ,  $\alpha \sim \mathcal{U}([1/48, 1/24])$ , and  $\beta_0 \sim \mathcal{TN}_{[0,1]}(0.4, 0.05^2)$ . For the DTHP model, the initial conditions were defined as  $\lambda_H(0) \sim \mathcal{U}(\{0, \dots, 15\})$ ,  $R_0 \sim \mathcal{N}(0.5, 0.05^2)$ , and  $\omega \sim \mathcal{U}([0, 1])$ . The hyperparameters were chosen as  $\nu_k \sim \mathcal{U}([0, 0.16])$  and  $\phi_k \sim \mathcal{U}([0, 0.2])$  for  $k = 1, 2$ .

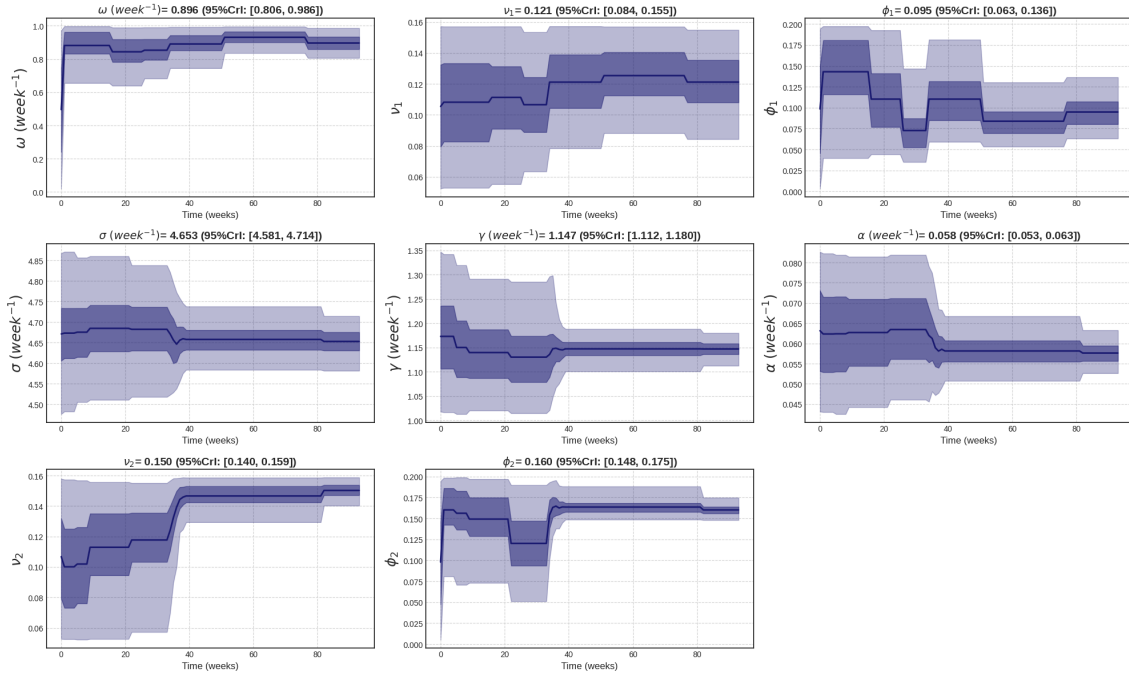


Figure C.1: Evolution of the weekly estimate of the posterior distributions of each parameter for the DTHP and SEIRS models obtained using  $\text{SMC}^2$  for Influenza data. Model posterior means are shown as dark violet lines, with the violet band representing the 95% credible intervals.

For COVID-19, we used the SEIR model with initial conditions specified as  $S(0) = N - E(0) - I(0)$ ,  $E(0) = 1$ ,  $I(0) \sim \mathcal{U}(\{0, \dots, 20\})$ , and  $R(0) = 0$ . The prior distributions were defined as  $\beta_0 \sim \mathcal{N}(0.5, 0.05^2)$ ,  $\sigma \sim \mathcal{TN}_{[1/5, 1/3]}(1/4, 0.1^2)$ , and  $\gamma \sim \mathcal{TN}_{[1/7.5, 1/4.5]}(1/6, 0.2^2)$ . For the DTHP model, the initial conditions were  $\lambda_H(0) \sim \mathcal{U}(\{0, \dots, 20\})$ ,  $R_0 \sim \mathcal{N}(3.2, 0.05^2)$ , and  $\omega \sim \mathcal{U}([0, 1])$ . The hyperparameters were set as  $\nu_k \sim \mathcal{TN}_{[0.05, 0.2]}(0.1, 0.01^2)$  and  $\phi_k \sim \mathcal{U}([0, 0.2])$  for  $k = 1, 2$ .

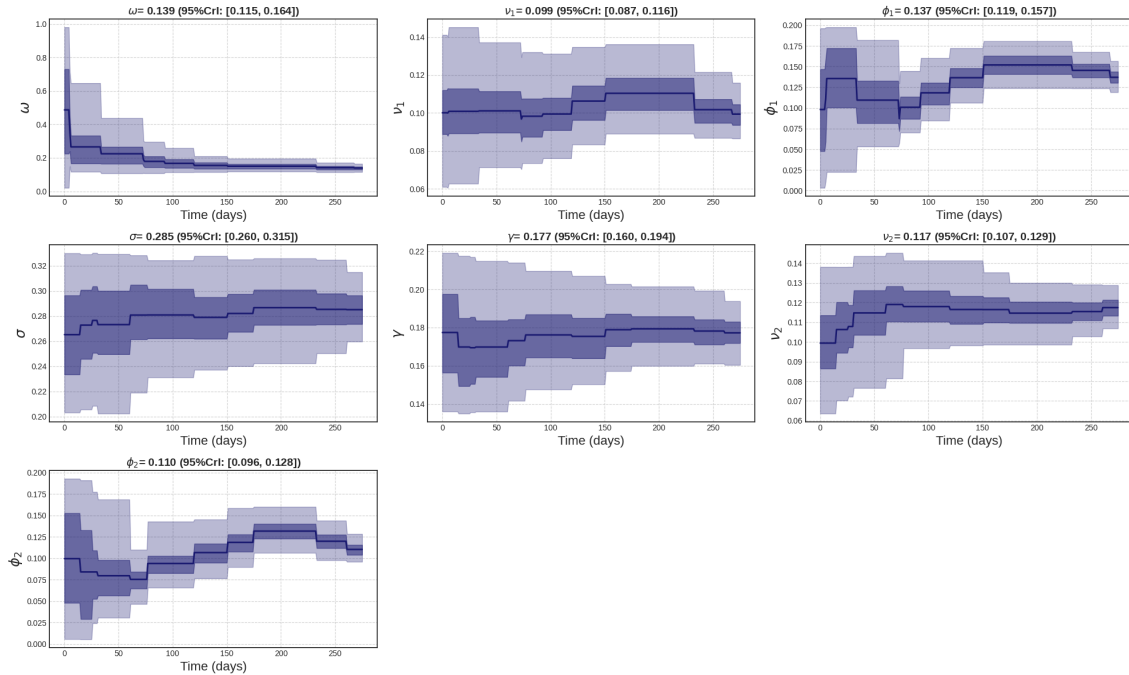


Figure C.2: Evolution of the daily estimate of the posterior distributions of each parameter for the DTHP and SEIR models obtained using  $\text{SMC}^2$  for COVID-19 data. Model posterior means are shown as dark violet lines, with the violet band representing the 95% credible intervals.

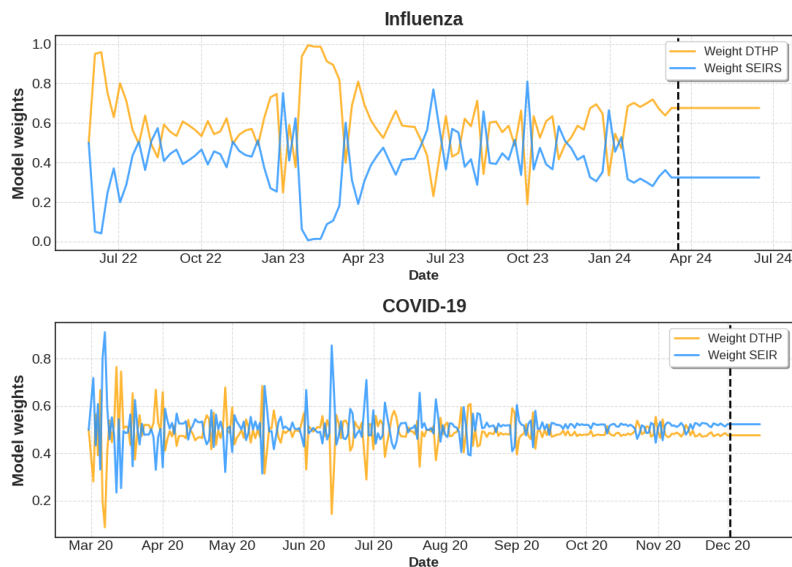


Figure C.3: **Evolution of model weights for the Influenza and COVID-19 Dataset.** The vertical black dashed line indicates the start of the forecasting period.

## References

- S. Abbott, J. Hellewell, R. N. Thompson, K. Sherratt, H. P. Gibbs, N. I. Bosse, J. D. Munday, S. Meakin, E. L. Doughty, J. Y. Chun, et al. Estimating the time-varying reproduction number of sars-cov-2 using national and subnational case counts. *Wellcome Open Research*, 5(112):112, 2020.
- C. Andrieu, A. Doucet, and R. Holenstein. Particle Markov Chain Monte Carlo Methods (with discussion). *Journal of the Royal Statistical Society: Series B (Statistical Methodology)*, 72(3):1–269, 2010.
- A. L. Bertozzi, E. Franco, G. Mohler, M. B. Short, and D. Sledge. The challenges of modeling and forecasting the spread of COVID-19.
- P. J. Birrell, R. G. Pebody, A. Charlett, X.-S. Zhang, and D. D. Angelis. Real-time modelling of a pandemic influenza outbreak. *Health Technology Assessment*, 21(58): 1–118, Oct 2017. doi: 10.3310/hta21580.
- P. J. Birrell, L. Wernisch, B. D. Tom, L. Held, G. O. Roberts, R. G. Pebody, and D. De Angelis. Efficient real-time monitoring of an emerging influenza pandemic: How feasible? *The annals of applied statistics*, 14(1):74, 2020.
- R. Browning, D. Sulem, K. Mengersen, V. Rivoirard, and J. Rousseau. Simple discrete-time self-exciting models can describe complex dynamic processes: A case study of COVID-19. *PLoS ONE*, 16(4):e0250015, 2021. doi: 10.1371/journal.pone.0250015. URL <https://doi.org/10.1371/journal.pone.0250015>.
- J. Castañeda and M. Aerts. Accounting for model selection uncertainty: Model averaging of prevalence and force of infection using fractional polynomials. *Revista Colombiana de Estadística*, 38(1):163–179, 2015.
- B. Cazelles, C. Champagne, B. Nguyen-Van-Yen, C. Comiskey, E. Vergu, and B. Roche. A mechanistic and data-driven reconstruction of the time-varying reproduction number: Application to the covid-19 epidemic. *PLoS computational biology*, 17(7):e1009211, 2021.
- W.-H. Chiang, X. Liu, and G. Mohler. Hawkes process modeling of COVID-19 with mobility leading indicators and spatial covariates. *International Journal of Forecasting*, 38(2):505–520, April-June 2022. doi: 10.1016/j.ijforecast.2021.07.001.

- N. Chopin and O. Papaspiliopoulos. *SMC<sup>2</sup>, Sequential Inference in State-Space Models*, pages 357–370. Springer International Publishing, Cham, 2020. ISBN 978-3-030-47845-2. doi: 10.1007/978-3-030-47845-2\_18. URL [https://doi.org/10.1007/978-3-030-47845-2\\_18](https://doi.org/10.1007/978-3-030-47845-2_18).
- N. Chopin, P. E. Jacob, and O. Papaspiliopoulos. SMC<sup>2</sup>: An Efficient Algorithm for Sequential Analysis of State Space Models. *Journal of the Royal Statistical Society: Series B (Statistical Methodology)*, 75:397–426, 2013.
- R. Douc and O. Cappé. Comparison of resampling schemes for particle filtering. In *ISPA 2005. Proceedings of the 4th International Symposium on Image and Signal Processing and Analysis, 2005.*, pages 64–69. IEEE, 2005.
- A. Doucet, N. De Freitas, and N. Gordon. An introduction to sequential monte carlo methods. *Sequential Monte Carlo methods in practice*, pages 3–14, 2001.
- J. Dureau, K. Kalogeropoulos, and M. Baguelin. Capturing the time-varying drivers of an epidemic using stochastic dynamical systems. *Biostatistics*, 14(3):541–555, July 2013. doi: 10.1093/biostatistics/kxs052. Epub 2013 Jan 4.
- J. H. Fowler, S. J. Hill, N. Obradovich, and R. Levin. The effect of stay-at-home orders on COVID-19 cases and fatalities in the United States. *medRxiv*, 5 2020.
- S. Funk, A. Camacho, A. J. Kucharski, R. M. Eggo, and W. J. Edmunds. Real-time forecasting of infectious disease dynamics with a stochastic semi-mechanistic model. *Epidemics*, 22:56–61, 2018.
- N. Gordon, D. Salmond, and A. Smith. Novel Approach to Nonlinear/Non-Gaussian Bayesian State Estimation. *IEEE Proceedings F – Radar and Signal Processing*, 140(2):107–113, 1993. doi: 10.1049/ip-f-2.1993.0015.
- R. J. Goudie, A. M. Presanis, D. Lunn, D. De Angelis, and L. Wernisch. Joining and splitting models with markov melding. *Bayesian analysis*, 14(1):81, 2019.
- A. G. Hawkes. Point spectra of some mutually exciting point processes. *Journal of the Royal Statistical Society. Series B (Methodological)*, 33:438–443, 1971.
- Health Protection Surveillance Centre. Seasonal influenza. <https://www.hpsc.ie/a-z/respiratory/influenza/seasonalinfluenza/>, 2024. Accessed: 2024-09-25.
- J. Hellewell, S. Abbott, A. Gimma, N. I. Bosse, C. I. Jarvis, T. W. Russell, and et al. Feasibility of controlling COVID-19 outbreaks by isolation of cases and contacts. *The Lancet Global Health*, 8(4):e488–e496, 2020.
- J. A. Hoeting, D. Madigan, A. E. Raftery, and C. T. Volinsky. Bayesian model averaging: a tutorial. *Statistical Science*, 14(4):382–417, 1999.
- H. Inouzhe, M. X. Rodríguez-Álvarez, L. Nagar, and E. Akhmatskaya. Dynamic SIR/SEIR-like models comprising a time-dependent transmission rate: Hamiltonian Monte Carlo approach with applications to COVID-19, 2023. URL <https://arxiv.org/abs/2301.06385>.
- P. E. Jacob, S. M. M. Alavi, A. Mahdi, S. J. Payne, and D. A. Howey. Bayesian inference in non-markovian state-space models with applications to battery fractional-order systems. *IEEE Transactions on Control Systems Technology*, 26(2):497–506, 2017.
- F.-Z. Jaouimaa, D. Dempsey, S. Van Osch, S. Kinsella, K. Burke, J. Wyse, and J. Sweeney. An age-structured seir model for covid-19 incidence in dublin, ireland with framework for evaluating health intervention cost. *Plos one*, 16(12):e0260632, 2021.

- A. Jordan, F. Krüger, and S. Lerch. Evaluating probabilistic forecasts with scoringrules. *Journal of Statistical Software*, 90:1–37, 2019.
- J. D. Kelly, J. Park, R. J. Harrigan, N. A. Hoff, S. D. Lee, R. Wannier, B. Selo, M. Mossoko, B. Njoloko, E. Okitolonda-Wemakoy, et al. Real-time predictions of the 2018–2019 ebola virus disease outbreak in the democratic republic of the congo using hawkes point process models. *Epidemics*, 28:100354, 2019.
- W. O. Kermack and A. G. McKendrick. A contribution to the mathematical theory of epidemics. *Proceedings of the Royal Society of London, Series A, Containing Papers of a Mathematical and Physical Character*, 115(772):700–721, 1927.
- S. Koyama, T. Horie, and S. Shinomoto. Estimating the time-varying reproduction number of COVID-19 with a state-space method. *PLoS Computational Biology*, 17:e1008679, 2021. doi: 10.1371/journal.pcbi.1008679.
- C. Kresin, F. Schoenberg, and G. Mohler. Comparison of hawkes and seir models for the spread of covid-19. *Advances and Applications in Statistics*, 74:83–106, 2021.
- S. Lamprinakou, A. Gandy, and E. McCoy. Using a latent Hawkes process for epidemiological modelling. *PLoS ONE*, 18(3):e0281370, 2023. doi: 10.1371/journal.pone.0281370. URL <https://doi.org/10.1371/journal.pone.0281370>.
- P. E. Lekone and B. F. Finkenstädt. Statistical inference in a stochastic epidemic seir model with control intervention: Ebola as a case study. *Biometrics*, 62(4):1170–1177, 2006.
- P. E. Lekone and B. F. Finkenstädt. Statistical inference in a stochastic epidemic SEIR model with control intervention: Ebola as a case study. *Biometrics*, 62(4):1170–1177, 2006.
- A. Lindén and S. Mäntyniemi. Using the negative binomial distribution to model overdispersion in ecological count data. *Ecology*, 92(7):1414–1421, 2011.
- L. Martino, J. Read, V. Elvira, and F. Louzada. Cooperative parallel particle filters for on-line model selection and applications to urban mobility. Tech. Rep. 1512.0420, viXra, 2015.
- S. Meyer and L. Held. Power-law models for infectious disease spread. *The Annals of Applied Statistics*, 8(3):1612–1639, September 2014. doi: 10.1214/14-AOAS743. URL <https://doi.org/10.1214/14-AOAS743>.
- G. Mohler, M. B. Short, F. Schoenberg, and D. Sledge. Analyzing the Impacts of Public Policy on COVID-19 Transmission: A Case Study of the Role of Model and Dataset Selection Using Data from Indiana. *Statistics and Public Policy*, 8(1):1–8, 2021. doi: 10.1080/2330443X.2020.1859030. URL <https://doi.org/10.1080/2330443X.2020.1859030>.
- J. Park, J. Goldstein, M. Haran, and M. Ferrari. An ensemble approach to predicting the impact of vaccination on rotavirus disease in niger. *Vaccine*, 35(43):5835–5841, 2017.
- J. Park, A. W. Chaffee, R. J. Harrigan, and F. P. Schoenberg. A non-parametric hawkes model of the spread of ebola in west africa. *Journal of Applied Statistics*, 49(3):621–637, 2022.
- M. A. Parrish, H. Moradkhani, and C. M. DeChant. Toward reduction of model uncertainty: Integration of bayesian model averaging and data assimilation. *Water Resources Research*, 48(3), 2012.

- J. Rings, J. A. Vrugt, G. Schoups, J. A. Huisman, and H. Vereecken. Bayesian model averaging using particle filtering and gaussian mixture modeling: Theory, concepts, and simulation experiments. *Water Resources Research*, 48(5), 2012.
- M.-A. Rizoiu, S. Mishra, Q. Kong, M. Carman, and L. Xie. IR-Hawkes: Linking epidemic models and Hawkes processes to model diffusions in finite populations. In *Proceedings Of The 2018 World Wide Web Conference*, pages 419–428, 2018. doi: 10.1145/3178876.3186108. URL <https://doi.org/10.1145/3178876.3186108>.
- G. Storvik, A. Diz-Lois Palomares, S. Engebretsen, G. Ø. I. Rø, K. Engø-Monsen, A. B. Kristoffersen, B. F. De Blasio, and A. Frigessi. A sequential Monte Carlo approach to estimate a time-varying reproduction number in infectious disease models: the Covid-19 case. *Journal of the Royal Statistical Society Series A: Statistics in Society*, 186(4): 616–632, 2023.
- I. Urteaga, M. F. Bugallo, and P. M. Djurić. Sequential Monte Carlo methods under model uncertainty. In *2016 IEEE Statistical Signal Processing Workshop (SSP)*, pages 1–5, Palma de Mallorca, Spain, 2016. doi: 10.1109/SSP.2016.7551747.
- R. M. Vieira. *Bayesian online state and parameter estimation for streaming data*. PhD thesis, Newcastle University, 2018.